Inorganic Chemistry

Article

pubs.acs.org/IC

Copper(II) Carboxylate Dimers Prepared from Ligands Designed to Form a Robust $\pi\cdots\pi$ Stacking Synthon: Supramolecular Structures and Molecular Properties

Daniel L. Reger,* Agota Debreczeni, and Mark D. Smith

Department of Chemistry and Biochemistry, University of South Carolina, Columbia, South Carolina 29208, United States

Julia Jezierska

Faculty of Chemistry, Wroclaw University, Wroclaw, Poland

Andrew Ozarowski*

National High Magnetic Field Laboratory, Florida State University, Tallahassee, Florida 32310 United States

Supporting Information

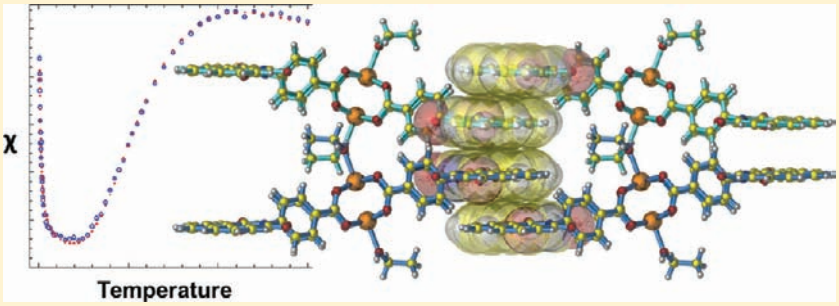

ABSTRACT: The reactions of bifunctional carboxylate ligands (1,8-naphthalimido)propanoate, ($\mathbf{L_{C2}}^-$), (1,8-naphthalimido)-ethanoate, ($\mathbf{L_{C1}}^-$), and (1,8-naphthalimido)benzoate, ($\mathbf{L_{C4}}^-$) with $Cu_2(O_2CCH_3)_4(H_2O)_2$ in methanol or ethanol at room temperature lead to the formation of novel dimeric $[Cu_2(\mathbf{L_{C2}})_4(MeOH)_2]$ (**1**), $[Cu_2(\mathbf{L_{C1}})_4(MeOH)_2]\cdot 2(CH_2Cl_2)$ (**2**), $[Cu_2(\mathbf{L_{C4}})_4(EtOH)_2]\cdot 2(CH_2Cl_2)$ (**3**) complexes. When the reaction of $\mathbf{L_{C1}}^-$ with $Cu_2(O_2CCH_3)_4(H_2O)_2$ was carried out at −20 °C in the presence of pyridine, $[Cu_2(\mathbf{L_{C1}})_4(py)_4]\cdot 2(CH_2Cl_2)$ (**4**) was produced. At the core of complexes **1**−**3** lies the square $Cu_2(O_2CR)_4$ "paddlewheel" secondary building unit, where the two copper centers have a nearly square pyramidal geometry with methanol or ethanol occupying the axial coordination sites. Complex **4** contains a different type of dimeric core generated by two κ^1-bridging carboxylate ligands. Additionally, two terminal carboxylates and four trans situated pyridine molecules complete the coordination environment of the five-coordinate copper(II) centers. In all four compounds, robust $\pi\cdots\pi$ stacking interactions of the naphthalimide rings organize the dimeric units into two-dimensional sheets. These two-dimensional networks are organized into a three-dimensional architecture by two different noncovalent interactions: strong $\pi\cdots\pi$ stacking of the naphthalimide rings (also the pyridine rings for **4**) in **1**, **3**, and **4**, and intermolecular hydrogen bonding of the coordinated methanol or ethanol molecules in **1**−**3**. Magnetic measurements show that the copper ions in the paddlewheel complexes **1**−**3** are strongly antiferromagnetically coupled with $-J$ values ranging from 255 to 325 cm^{-1}, whereas the copper ions in **4** are only weakly antiferromagnetically coupled. Typical values of the zero-field splitting parameter D were found from EPR studies of **1**−**3** and the related known complexes $[Cu_2(\mathbf{L_{C2}})_4(py)_2]\cdot 2(CH_2Cl_2)\cdot(CH_3OH)$, $[Cu_2(\mathbf{L_{C3}})_4(py)_2]\cdot 2(CH_2Cl_2)$ and $[Cu_2(\mathbf{L_{C3}})_4(bipy)]\cdot(CH_3OH)_2\cdot(CH_2Cl_2)_{3.37}$ ($\mathbf{L_{C3}}^-$ = (1,8-naphthalimido)butanoate)), while its abnormal magnitude in $[Cu_2(\mathbf{L_{C2}})_4(bipy)]$ was qualitatively rationalized by structural analysis and DFT calculations.

INTRODUCTION

Crystal engineering of metal−organic architectures with various properties, functions, and promising applications in catalysis,[1] energy storage,[2] sensing,[3] and separation[4] has become of great interest in the field of chemistry and materials science. The synthesis of metal−organic framework materials (MOFs) using the principles of coordination chemistry represents unique possibilities to combine the desirable properties of the individual organic and inorganic components.

Received: October 11, 2011
Published: December 27, 2011

   dx.doi.org/10.1021/ic202198k | *Inorg. Chem.* 2012, 51, 1068−1083

A wide variety of diverse architectures, with high structural stability, have been prepared by connecting rigid metallic building blocks, referred as secondary building units (SBUs), with robust organic linkers via strong covalent bonds. The use of multidentate carboxylate ligands as the robust organic linkers to join the metallic SBU cores has been studied extensively, with a particular advantage in many cases that neutral networks can be produced in which no counterions are needed to achieve electroneutrality.[5]

Less rigid, but still highly organized structures can be assembled by noncovalent supramolecular interactions. Hydrogen bonding is the most predominant organizational synthon in the design of supramolecular networks due to its clearly defined, reproducible and transferable directionality properties.[6] Another interaction which has gained increasing attention in the past few years is the $\pi\cdots\pi$ stacking interaction between aromatic rings. Although this interaction is not as directional as hydrogen bonding, an order of stability in the interaction of two π systems was well established: π-deficient − π-deficient > π-deficient − π-rich > π-rich − π-rich.[7] The interaction between π-donor and π-acceptor systems in the self-assembly process of organic molecules was exploited for the benefit of crystal engineering by several authors.[7d,e] Less attention has been dedicated to the $\pi\cdots\pi$ stacking interactions present in metal−organic supramolecular networks.

In the past few years we have focused on exploiting the $\pi\cdots\pi$ stacking capabilities of the π-deficient, 1,8-naphthalimide supramolecular synthon. By incorporating this moiety into bis(pyrazolyl)methane and 2,2′-bipyridine systems of ligands, we have shown that $\pi\cdots\pi$ stacking interactions between the 1,8-naphthalimide rings do not just organize the solid state structures, but also persist in solution.[8]

More recently, we have prepared bifunctional carboxylate ligands (Scheme 1) that contained both the carboxylate donor group and the 1,8-naphthalimide π-stacking group (tecton), in order to assemble MOF type architectures that are organized by noncovalent forces.[9] We have termed these solids supramolecular metal−organic frameworks (SMOFs), framework solids with a three-dimensional structure in which the building blocks are organized partially or completely by robust supramolecular interactions.

Scheme 1. Bifunctional Carboxylate Ligands

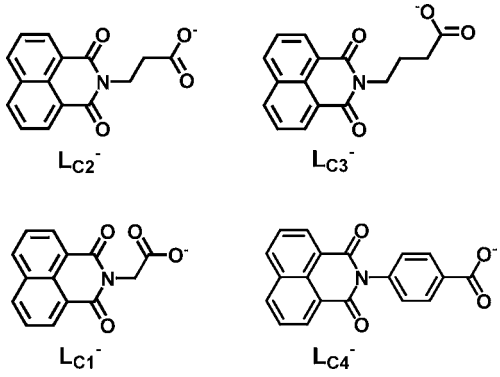

In our original work, two carboxylate ligands (L_{C2}^- and L_{C3}^-) were prepared and incorporated into the paddlewheel $Cu_2(O_2CR)_4$ type SBU.[9a] Four compounds with the general formula $Cu_2(O_2CR)_4(L)_2$ (where L = pyridine or 4,4′-bipyridine) were prepared, all four being organized partially or completely by the $\pi\cdots\pi$ stacking of the 1,8-naphthalimide rings into high-dimensionality materials. The dicopper tetracarboxylate system was of interest not just because of the appealing "square" architecture of the $Cu_2(O_2CR)_4$ SBU core and the strong axial ligation provided by the copper(II) ions, but also because paddlewheel dicopper tetracarboxylates are known to exhibit very strong antiferromagnetic interaction between the unpaired electrons of the d^9 copper(II) centers.[10] Factors affecting the magnitude and character of the exchange interactions in bridged binuclear transition metal complexes have been of particular interest.[11−13]

In our efforts to develop more fully the structural trends with this class of bifunctional ligands, we have carried out two important types of ligand modifications and prepared and investigated the properties of new paddlewheel $Cu_2(O_2CR)_4$ type complexes to more deeply probe how the 1,8-naphthalimide rings enter into different types of $\pi\cdots\pi$ stacking interactions under various structural situations. First, we have changed the length and rigidity of the link between the carboxylate donor group and the 1,8-naphthalimide ring by the synthesis of two new carboxylate ligands (L_{C1}^- and L_{C4}^-; see Scheme 1). Second, we have replaced the nitrogen based pyridine at the axial position with the oxygen based ligands methanol or ethanol, ligands that can also enter into hydrogen bonding interactions. In addition, we have more completely characterized the complexes with a combination of magnetic and EPR studies and DFT calculations.

EXPERIMENTAL SECTION

General Considerations. All reactants were used as purchased from Aldrich. The synthesis of the protonated forms of the ligands, HL_{C1}, HL_{C2}, and HL_{C4}, have been reported elsewhere.[14] Elemental analyses were performed by Robertson Microlit Laboratories (Ledgewood, NJ). Thermogravimetric analysis was performed using a Thermal Analysis (TA) SDT-Q600 simultaneous DTA/TGA system. The samples were heated in air to 800 °C with a heating rate of 10 °C/min. The reflectance measurements were done on a Perkin-Elmer Lambda 35 UV−vis spectrometer using the Labsphere RSA-PE-20 Reflectance Spectroscopy Accessory. Microcrystalline samples were used in 4 mm cell.

Synthesis of $[Cu_2(L_{C2})_4(MeOH)_2]$ (1). HL_{C2} (0.054 g, 0.20 mmol) was dissolved in dichloromethane (20 mL). $Cu_2(O_2CCH_3)_4(H_2O)_2$ (0.021 g, 0.052 mmol) was dissolved in methanol (20 mL). Equal aliquots of each solution were divided into three test tubes (dichloromethane solution added first) with a buffer layer of pure methanol placed between the two solutions. The test tubes were stored undisturbed at room temperature. After a few days, dark blue X-ray quality crystals were obtained. Yield: 0.049 g (0.039 mmol, 74%). The analytical sample was dried to constant weight, Anal. Calcd. (Found) for $C_{62}H_{48}Cu_2N_4O_{18}$: C 58.91 (58.45); H 3.83 (3.80); N 4.43 (4.29). The reflectance spectrum shows two bands having maxima at 372 nm (band II) and at 708 nm (band I).

Synthesis of $[Cu_2(L_{C1})_4(MeOH)_2]\cdot 2(CH_2Cl_2)$ (2). This compound was prepared by the same procedure as $[Cu_2(L_{C2})_4(MeOH)_2]$. HL_{C1} (0.051 g, 0.20 mmol) and $Cu_2(O_2CCH_3)_4(H_2O)_2$ (0.021 g, 0.052 mmol) were used for synthesis. Yield: 0.044 g (0.032 mmol, 61%). The analytical sample was dried to constant weight, Anal. Calcd. (Found) for $C_{58}H_{40}Cu_2N_4O_{18}$ (without solvent): C 57.67 (57.68); H 3.34 (3.09); N 4.64 (4.81). The reflectance spectrum shows two bands having maxima at 378 nm (band II) and at 710 nm (band I).

Synthesis of $[Cu_2(L_{C4})_4(EtOH)_2]\cdot 2(CH_2Cl_2)$ (3). This compound was prepared by the same procedure as $[Cu_2(L_{C2})_4(MeOH)_2]$. The $Cu_2(O_2CCH_3)_4(H_2O)_2$ (0.021 g, 0.052 mmol) was dissolved in ethanol (20 mL) instead of methanol, and 12 drops of pyridine were added to the dichloromethane solution of HL_{C4} (0.064 g, 0.20 mmol). Yield: 0.050 g (0.030 mmol, 57%). Anal. Calcd. (Found)

dx.doi.org/10.1021/ic202198k | Inorg. Chem. 2012, 51, 1068−1083

Table 1. Selected Crystallographic Data for $[Cu_2(L_{C2})_4(MeOH)_2]$ (1), $[Cu_2(L_{C1})_4(MeOH)_2]\cdot 2(CH_2Cl_2)$ (2), $[Cu_2(L_{C4})_4(EtOH)_2]\cdot 2(CH_2Cl_2)$ (3), and $[Cu_2(L_{C1})_4(py)_4]\cdot 2(CH_2Cl_2)$ (4)

	1	2	3	4
formula	$C_{62}H_{48}Cu_2N_4O_{18}$	$C_{60}H_{44}Cl_4Cu_2N_4O_{18}$	$C_{82}H_{56}Cl_4Cu_2N_4O_{18}$	$C_{78}H_{56}Cl_4Cu_2N_8O_{16}$
fw, g mol^{-1}	1264.12	1377.87	1654.19	1630.19
cryst syst	monoclinic	monoclinic	monoclinic	triclinic
space group	$P2_1/c$	$P2_1/c$	C 2/c	P $\bar{1}$
T (K)	150(2)	150(2)	150(2)	150(2)
a, Å	7.4244(4)	7.5527(4)	28.2716(17)	10.5476(5)
b, Å	22.7983(11)	19.5974(11)	18.4654(11)	11.9372(5)
c, Å	16.0071(8)	18.7062(10)	13.5350(8)	14.8309(7)
α, deg	90	90	90	77.983(1)
β, deg	100.108(1)	97.212(1)	96.852(1)	74.524(1)
γ, deg	90	90	90	82.625(1)
V, Å^3	2667.4(2)	2746.9(3)	7015.4(7)	1754.94(14)
Z	2	2	4	1
R_1 $[I > 2\sigma(I)]$	0.0422	0.0477	0.0488	0.0507
wR_2 $[I > 2\sigma(I)]$	0.0793	0.1176	0.1120	0.1371

for $C_{82}H_{56}Cl_4Cu_2N_4O_{18}$: C 59.54 (58.39); H 3.41 (3.54); N 3.39 (3.41). The reflectance spectrum shows two bands having maxima at 422 nm (band II) and at 727 nm (band I).

Synthesis of $[Cu_2(L_{C1})_4(py)_4]\cdot 2(CH_2Cl_2)$ (4). This compound was prepared by the same procedure as $[Cu_2(L_{C1})_4(MeOH)_2]\cdot 2(CH_2Cl_2)$ using the same amount of starting materials, but in this case 12 drops of pyridine was added to the dichloromethane solution of HL_{C1} and the test tubes were placed in a −20 °C freezer. After a few weeks, dark blue X-ray quality crystals were obtained. Yield: 0.059 g (0.036 mmol, 69%). Anal. Calcd (Found) for $C_{78}H_{56}Cl_4Cu_2N_8O_{16}$: C 57.47 (57.49); H 3.46 (3.50); N 6.87 (6.89). The reflectance spectrum shows two bands having maxima at 371 nm (band II) and at 617 nm (band I).

Magnetic Properties. Magnetic susceptibility data of powdered samples were measured with a SQUID magnetometer (Quantum Design MPMSXL-5, Faculty of Chemistry, Wroclaw University) over the temperature range 1.8−300 K at the magnetic induction of 0.5 T. Corrections for the sample holders were applied. Diamagnetic corrections were determined from Pascal's constants.[15]

EPR Spectra. High-field, high-frequency EPR spectra at temperatures ranging from ∼3−300 K were recorded on a home-built spectrometer at the EMR facility of NHMFL.[16] The instrument was a transmission-type device in which microwaves are propagated in cylindrical lightpipes. The microwaves were generated by a phase-locked Virginia Diodes source generating frequency of 13 ± 1 GHz and producing its harmonics of which the second, fourth, sixth, eighth, 16th, 24th and 32nd were available. No resonance cavity was used. A superconducting magnet (Oxford Instruments) capable of reaching a field of 17 T was employed. Additionally, X-band (9.8 GHz) and Q-Band spectra (34 GHz) were recorded for some of the compounds on a Bruker ElexSys E500 instrument equipped with an NMR teslameter ER 036TM and a frequency counter E 41 FC (Chemistry, Wroclaw University).

Crystallographic Studies. For all the complexes, X-ray diffraction intensity data was measured at 150(2) K on a Bruker SMART APEX CCD-based diffractometer system (Mo Kα radiation, λ = 0.71073 Å). Raw area detector data frame integration was performed with SAINT+.[17] Direct methods structure solution, difference Fourier calculations and full-matrix least-squares refinement against F^2 were performed with SHELXTL.[18] All non-hydrogen atoms were refined with anisotropic displacement parameters except where noted. Hydrogen atoms bonded to carbon atoms were located in difference maps before being placed in geometrically idealized positions and included as riding atoms. Details of the data collection are given in Table 1, while further details regarding the solution and refinement of the structures are presented in the Supporting Information.

RESULTS

The copper(II) complexes of three carboxylate ligands (L_{C2}^-, L_{C1}^-, L_{C4}^-) using alcohols as the axial ligand were prepared by layering technique. Onto a dichloromethane solution of the acid form of the carboxylate ligand pure methanol (ethanol for **3**) was layered, and then a methanol (ethanol for **3**) solution of $Cu_2(O_2CCH_3)_4(H_2O)_2$ was added as the third layer. After a few days, green or blue X-ray quality crystals of $[Cu_2(L_{C2})_4(MeOH)_2]$ (**1**), $[Cu_2(L_{C1})_4(MeOH)_2]\cdot 2(CH_2Cl_2)$ (**2**), and $[Cu_2(L_{C4})_4(EtOH)_2]\cdot 2(CH_2Cl_2)$ (**3**) were obtained. The reaction of L_{C1}^- with $Cu_2(O_2CCH_3)_4(H_2O)_2$ at room temperature containing small amounts of pyridine also led to the formation of complex **2**, but in this case the crystallization requires a few weeks rather than a few days as in the absence of pyridine. If these layered solutions containing small amounts of pyridine are stored in a freezer (−20 °C), using these same amounts of starting materials that produce **2** at ambient temperature, $[Cu_2(L_{C1})_4(py)_4]\cdot 2(CH_2Cl_2)$ (**4**) is obtained. The important factor in the formation of **4** over **2** is the lower temperature of the crystallization procedure.

Solid State Structure Analysis. Selected bond lengths and angles are gathered in Supporting Information Table S1. The core of three complexes reported here (**1**-**3**) is the square, dimeric $Cu_2(O_2CR)_4$ "paddlewheel" SBU structural motif. The nonbonding Cu···Cu distances are between 2.60 and 2.64 Å. Ethanol was used as the axial ligand for **3** because it did not prove possible to obtain X-ray quality crystals of the analogous methanol complex. The structure of **4** is also dimeric, but it is not formed from a paddlewheel SBU.

Figure 1 shows a structural diagram for $[Cu_2(L_{C2})_4(MeOH)_2]$ (**1**). Four carboxylate groups from four separate ligands bridge the two copper(II) ions in κ^2 fashion placing the oxygen donor atoms at the equatorial positions of the square pyramidal, five-coordinate copper(II) centers. The remaining axial site on each copper(II) ion is completed by a methanol molecule.

Robust $\pi\cdots\pi$ stacking of the electron-deficient 1,8-naphthalimide groups from the carboxylate ligands and intermolecular hydrogen bonding of the coordinated methanol molecules organize **1** into a three-dimensional supramolecular architecture. Each naphthalimide moiety of the dimetallic unit $\pi\cdots\pi$ stacks with naphthalimide groups of adjacent dinuclear SBUs generating a two-dimensional sheet oriented in approximately the same dimension as the square plane formed

dx.doi.org/10.1021/ic202198k | Inorg. Chem. 2012, 51, 1068−1083

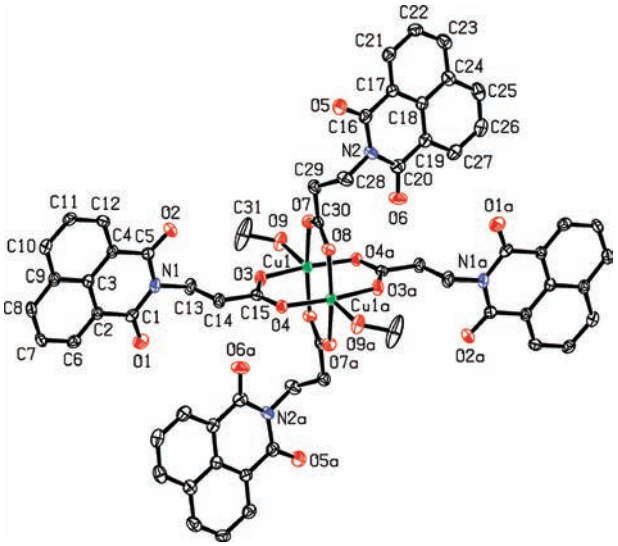

Figure 1. Molecular structure of $[Cu_2(L_{C2})_4(MeOH)_2]$ (**1**).

by the carboxylate carbon atoms of the dimeric SBU cores, Figure 2. For each SBU there are two types of ligands with different orientations of the alkyl spacers; two of them are "linear" and the other two are "bent" when observed along the MeOH−Cu···Cu−MeOH axis (see Figure 2). Within this two-dimensional network the two types of ligands participate in $\pi\cdots\pi$ stacking interactions that have similar metric parameters. The "linear" ligands from the central green-colored dimeric unit in Figure 2 $\pi\cdots\pi$ stack with the "bent" ligands from the neighboring blue-colored units, with a perpendicular distance between the rings of 3.42 Å. The dipole vectors of the naphthalimide rings (running from the center of the fused rings through the nitrogen atom) are oriented at 92° and the angle between the planes of the rings is 2.7°. The interactions between the "bent" ligands from the central green dimeric unit and the "linear" ligands from the blue neighboring units have similar metrics.

In our earlier work, we introduced a parameter, χ, to quantify the amount of slippage one ring involved in the $\pi\cdots\pi$ stack has with respect to the other.[9a] The parameter is the third side of the right triangle formed with the average perpendicular distance between the rings and the line joining the central carbon atoms of the two rings. In this two-dimensional structure of **1**, the slippage values for the naphthalimide rings are 1.47 and 1.51 Å, values in the range of strong interactions (0.25−2.4 Å) as previously reported.[9,14]

The $\pi\cdots\pi$ stacking interactions between the naphthalimide rings of the two different types of ligands continue in the third dimension (crystallographic *a* axis direction) linking the sheets into a three-dimensional architecture. Figure 3 shows two sheets edge on connected by these $\pi\cdots\pi$ stacking interactions of the naphthalimide rings.

Additionally, there are intermolecular hydrogen bonding interactions between the coordinated methanol molecules that support the three-dimensional architecture. The main hydrogen bonding interactions (shown as red dots in Figure 3) are formed between the hydrogen atoms of the methanol axial ligands and one of the four bridging carboxylate oxygen atoms of the dimeric unit from the next sheet. In this interaction, the H···O distance is 1.97(3) Å with an OHO angle of 163°. There are also weaker C−H···O interactions within and between the sheets, shown as light blue dots in Figure 3. In these C−H···O interactions between the hydrogen atom on the naphthalimide ring and the oxygen atom of a bridging carboxylate, the H···O distance is 2.37(6) Å with a CHO angle of 169°.

The solid state structure of **2** is shown in Figure 4. The square, dimeric $Cu_2(O_2CR)_4$ core retains the basic "copper acetate dimer" arrangement, with an axial methanol completing the square pyramidal geometry about each five-coordinate copper(II) ion, but the shortening of the alkyl spacer between the naphthalimide unit and the carboxylate to a single CH_2 group has a dramatic impact on the orientation of the naphthalimide rings. The side arms of all four carboxylate ligands are "bent" and cannot follow the "square" arrangement imposed by the SBU core; the naphthalimide groups are

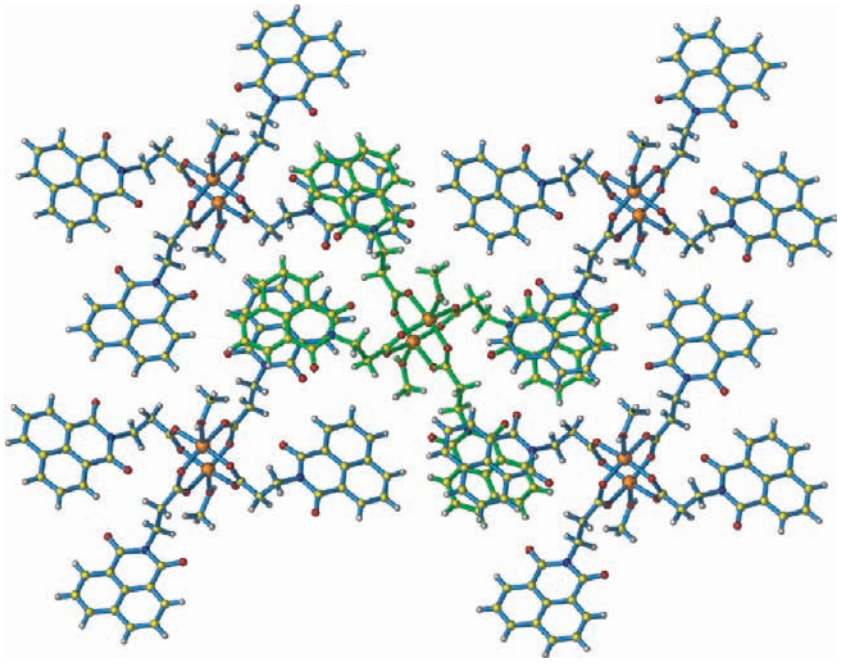

Figure 2. Two-dimensional structure of **1**. One central $[Cu_2(L_{C2})_4(MeOH)_2]$ molecule (green) and four adjacent dimeric units (blue) are shown.

dx.doi.org/10.1021/ic202198k | *Inorg. Chem.* 2012, 51, 1068−1083

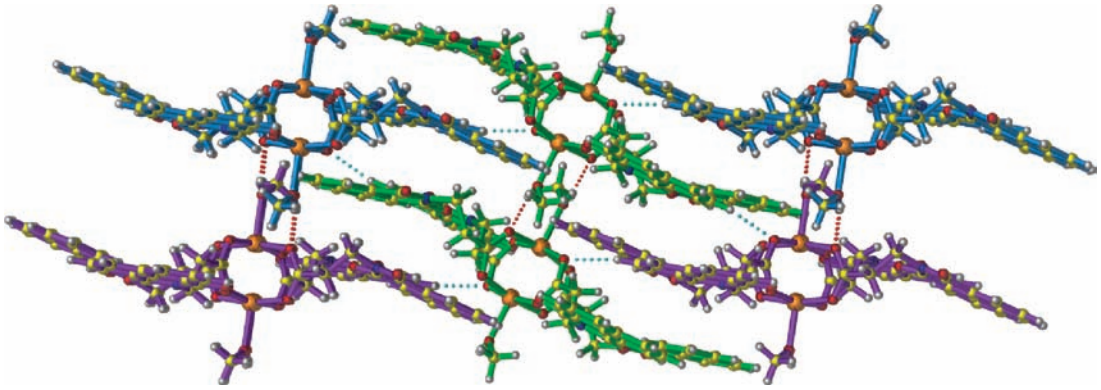

Figure 3. Three-dimensional structure of **1**. Two sheets are shown: the top sheet with blue and green bonds is as pictured in Figure 2, but rotated by 90° in the horizontal direction. The red dots represent the hydrogen bonds, which link the two sheets together, along with the $\pi\cdots\pi$ stacking interactions between the naphthalimide rings of the two separate sheets. The light blue dots mark the weaker intra and intersheet C−H···O interactions.

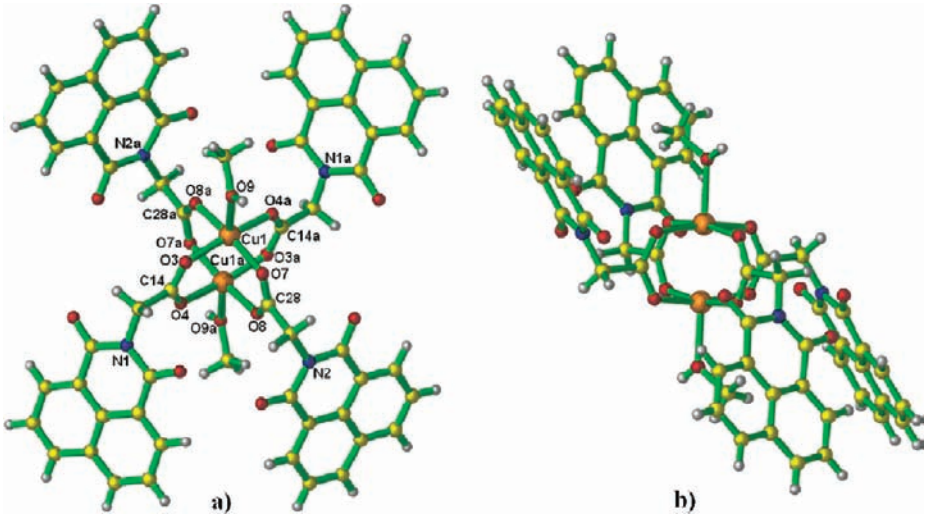

Figure 4. (a) Molecular structure of $[Cu_2(\mathbf{L}_{C1})_4(MeOH)_2]\cdot 2(CH_2Cl_2)$ (**2**). (b) Same structure as in a rotated by approximately 45°.

arranged such that two adjacent rings are located on each side of the square paddlewheel unit (Figure 4b).

Despite the difference in orientation of the naphthalimide rings with respect to the dimeric core when comparing **2** with **1**, again each naphthalimide ring of the dimeric units $\pi\cdots\pi$ stacks with naphthalimide groups of adjacent dinuclear SBUs generating a two-dimensional sheet structure, Figure 5. In this case, the $\pi\cdots\pi$ stacking interactions are approximately perpendicular to the square plane formed by the carboxylate carbon atoms of the dimeric SBU cores. In all of these interactions the naphthalimide ring distance is 3.35 Å, the rings are almost parallel with an interplanar angle of 1.7° and the dipole vectors of the naphthalimide units are oriented at 136°. The relatively small χ value of 1.08 Å coupled with the above metrics indicates strong interactions.

The two-dimensional sheets are connected into a three-dimensional architecture by the intermolecular hydrogen bonding of the coordinated methanol molecules. In Figure 6a the hydrogen bonds between two dimeric units of two separate sheets are pictured. The coordinated methanol molecules are hydrogen bonded with the carbonyl oxygen atom of the naphthalimide rings from adjacent dimeric units. In this interaction, the H···O distance is 2.03 Å with an OHO angle of 170°. There are also weaker C−H···O interactions between the sheets shown in Figure 6b. In these interactions, the H···O distances are 2.54 and 2.74 Å, respectively, with a CHO angle of 154° and 155°. In contrast to compound **1**, the orientation of the naphthalimide groups prevent $\pi\cdots\pi$ stacking interactions from forming in this third dimension.

The molecular structure of **3** is pictured in Figure 7. As in the previous compounds, the "paddlewheel" motif is present in **3**. The rigid phenylene arms of the ligand are directed in the four directions implanted by the "square" SBU core and are oriented nearly in the same plane as the carboxylate functional group and at an average angle of 69° to the naphthalimide rings.

Three different types of $\pi\cdots\pi$ stacking interactions of the naphthalimide groups organize the dimeric SBUs into a three-dimensional network. As illustrated in the middle of Figure 8a, three types of $\pi\cdots\pi$ stacking interactions are formed between four naphthalimide rings of adjacent dimeric units: the first type of $\pi\cdots\pi$ stacking is formed between rings colored the same, both the two light blue colored and the two dark blue colored rings (A), the second is formed between a light blue and a dark blue ring (B), and the third one is also between a dark blue ring and a light blue ring (C), but has different parameters from B. The parameters for the A, B, and C interactions are as

dx.doi.org/10.1021/ic202198k | *Inorg. Chem.* 2012, 51, 1068−1083

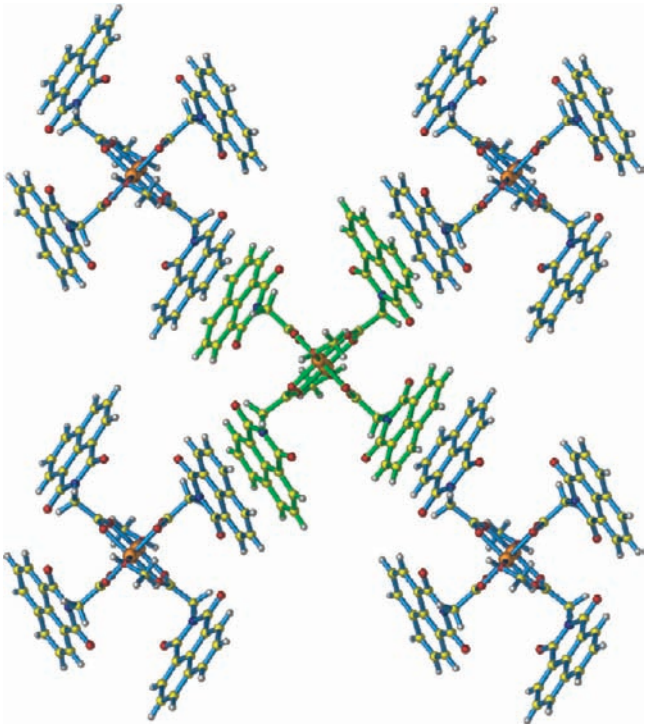

Figure 5. Two-dimensional structure of **2**. View down the MeOH–Cu···Cu–MeOH axis of the $\pi\cdots\pi$ stacking interactions of the naphthalimide rings.

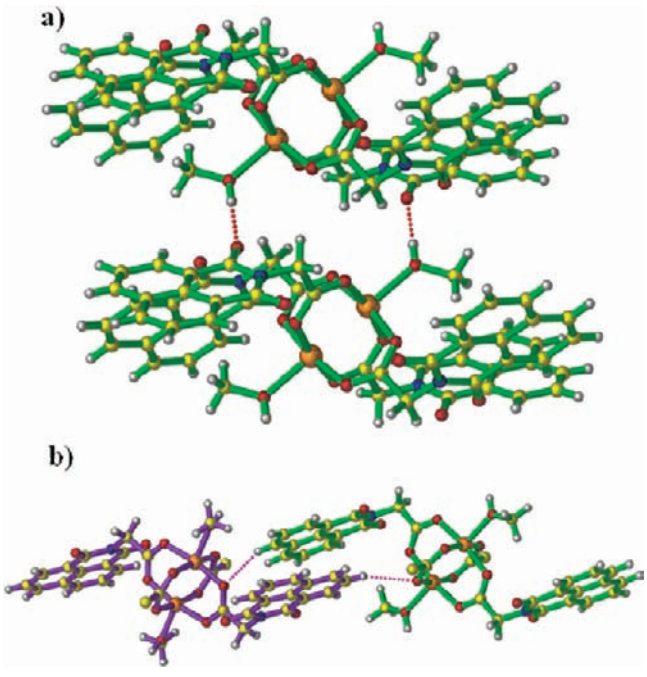

Figure 6. (a) Strong O–H···O hydrogen bonding interactions in **2** represented by red dots. (b) Weaker C–H···O interactions in **2** shown by purple dots.

follows: the naphthalimide rings are 3.42, 3.32, and 3.39 Å apart, the rings are nearly parallel and the dipole vectors of the naphthalimide units are oriented at 96°, 80°, and 76°, respectively. The slippage parameter values indicate strong interactions in all cases (χ is 1.47 Å 1.19 Å, and 0.15 Å). Along the crystallographic *c* axis, the dimeric units are assembled in an

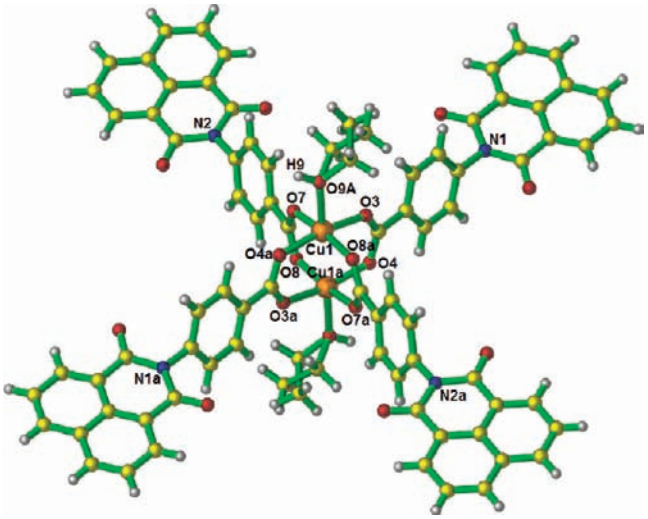

Figure 7. Molecular structure of $[Cu_2(L_{C4})_4(EtOH)_2]\cdot 2(CH_2Cl_2)$ (**3**). The axial ethanol ligands are disordered over two sites.

ABAC fashion into a three-dimensional network by these $\pi\cdots\pi$ stacking interactions. Figure 8b shows the same dimeric units as Figure 8a, but rotated 90°, illustrating the open three-dimensional network structure of **3**.

In the structure of **3**, there are two of these symmetry equivalent networks, which interpenetrate generating a 2-fold interpenetrated three-dimensional architecture. Figure 9 shows the blue-colored network from Figure 8b interpenetrated with the second, purple-colored network. The light and dark colors delineate six dimers within each network. While in the first network the dimeric units are π-stacked in an ABAC fashion, the dimeric units of the second network are assembled in an ACAB fashion by the $\pi\cdots\pi$ stacking interactions along the *c* crystallographic axis.

The two interpenetrated networks are connected by intermolecular hydrogen bonding of the axial ethanol molecules, indicated in Figure 9 by the green dots. In these interactions, the coordinated ethanol molecules from one network are hydrogen bonded with the carbonyl oxygen atom of naphthalimide rings from the second network. The H···O distance is 1.99 Å with an OHO angle of 159°.

A molecular diagram of **4** is shown in Figure 10. In contrast to the previous compounds, in **4** the two equivalent copper(II) ions are linked by two μ-κ^1-carboxylate ligands to form a centrosymmetric copper dimer, which does not contain the "paddlewheel" motif. The four equatorial positions of the square pyramidal, five-coordinate copper(II) centers are occupied by the oxygen atom of the bridging κ^1-carboxylate, the oxygen atom of a terminal carboxylate and the nitrogen atoms of two trans oriented pyridine molecules. The axial position of each copper center is occupied by the oxygen atom of the symmetry equivalent bridging κ^1-carboxylate ligand.

The Cu(1)–O(3a) axial distance is significantly longer than the other Cu(1)–O(3) distance [2.381(2) Å vs 1.972(2) Å]. The Cu(1)–O(3)–Cu(1a) angle is 101.61(8)°, which is in the range of 96.1–103.0° for other dimeric copper(II) complexes[19] with two carboxylato ligands bridging through a single oxygen. Consequently, in **4** the Cu···Cu distance is much longer than the Cu···Cu distance in the paddlewheel complexes [3.38 Å vs 2.6–2.7 Å]. In this new dimeric core, the two copper centers and all four carboxylato groups are situated in the same plane.

dx.doi.org/10.1021/ic202198k | *Inorg. Chem.* 2012, 51, 1068–1083

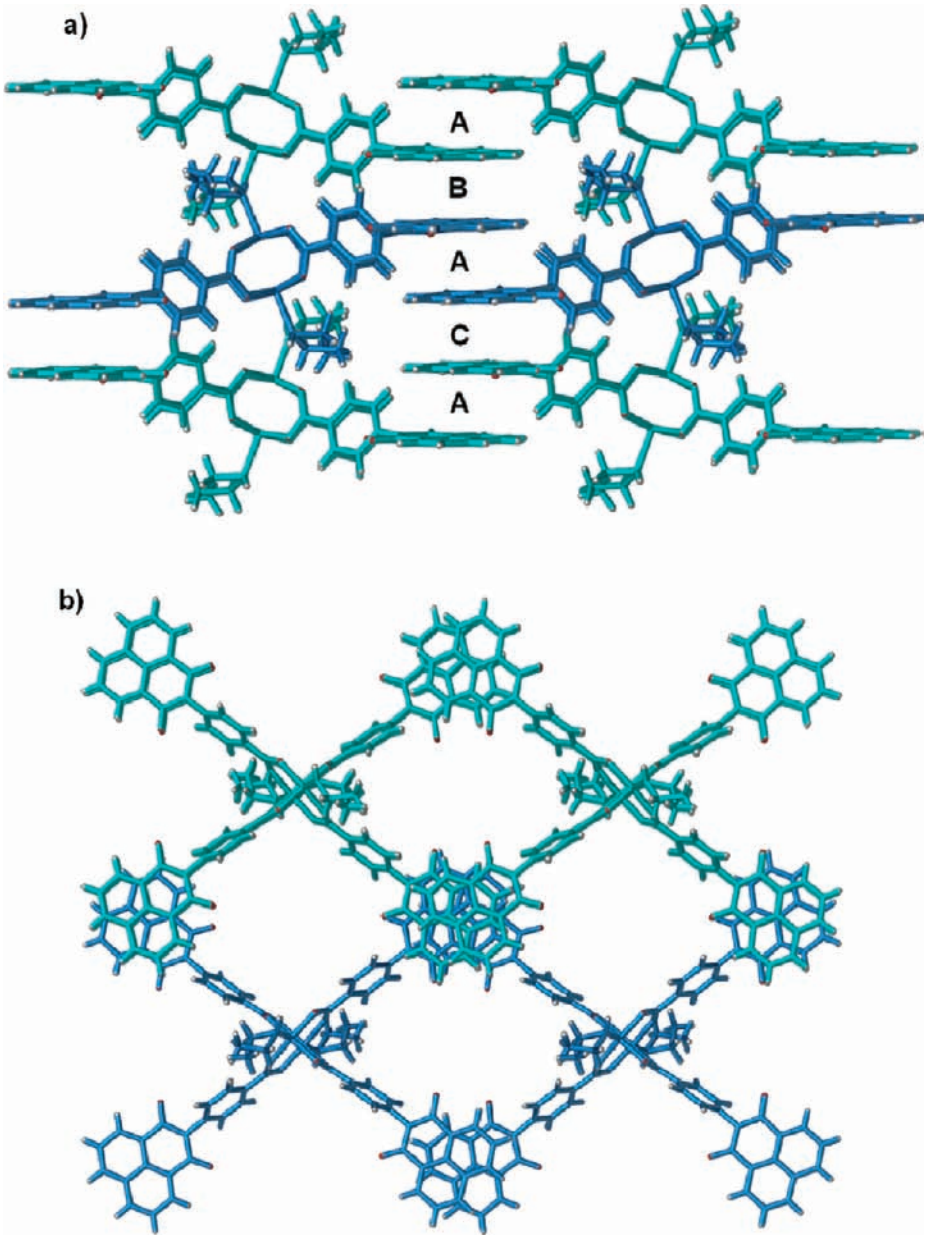

Figure 8. (a) Three pairs of stacked dimeric units in **3** generating a three-dimensional network. (b) The same dimeric units are shown as in a, but rotated 90°.

The naphthalimide rings are arranged such that two adjacent rings are located on each side of this planar dimeric unit.

Each naphthalimide moiety participates in two types of $\pi\cdots\pi$ stacking interactions. In one type, the κ^1-type bonding of both the bridging and terminal carboxylic groups allows the arms to orient the naphthalimide rings in positions that can form intramolecular $\pi\cdots\pi$ stacking. Despite the short perpendicular distance of 3.38 Å, the naphthalimide rings are slipped in this intramolecular interaction with a χ value of 2.45 Å indicating a weaker interaction. In the other type of interaction, each naphthalimide ring $\pi\cdots\pi$ stacks with a naphthalimide ring from the adjacent dimeric units generating a two-dimensional sheet structure oriented approximately in the same dimension as the plane of the dimeric units (Figure 11). This intermolecular $\pi\cdots\pi$ stacking is a strong interaction with a 3.44 Å distance between the nearly parallel rings, and a χ value of 1.10 Å. The naphthalimide-naphthalimide dipole vector angle is 180°.

The pyridine rings also enter into $\pi\cdots\pi$ stacking interactions. Two coordinated pyridine rings of two dimers from two separate sheets participate in intermolecular $\pi\cdots\pi$ stacking, as shown in Figure 12. The rings containing the N4 and N4a atoms are involved in $\pi\cdots\pi$ stacking indicated by the purple dots in Figure 12 with a perpendicular distance between the parallel rings of 3.42 Å. The distance between the centroids of the other two rings containing the N3 and N3a atoms is 4.38 Å, thus these rings are not in the range of intermolecular $\pi\cdots\pi$ stacking.[7a] However, there are intramolecular $\pi\cdots\pi$ stacking interactions between the rings containing the N3 and N4 atoms (marked by the light blue dots) with the perpendicular distance between the rings of 3.63 Å.

The intermolecular $\pi\cdots\pi$ stacking interactions of the pyridine rings build the structure into the third dimension. Two sheets, one colored green, rotated 90° from that in Figure 11, and one colored blue are shown in Figure 13. The $\pi\cdots\pi$ stacking of

dx.doi.org/10.1021/ic202198k | *Inorg. Chem.* 2012, 51, 1068–1083

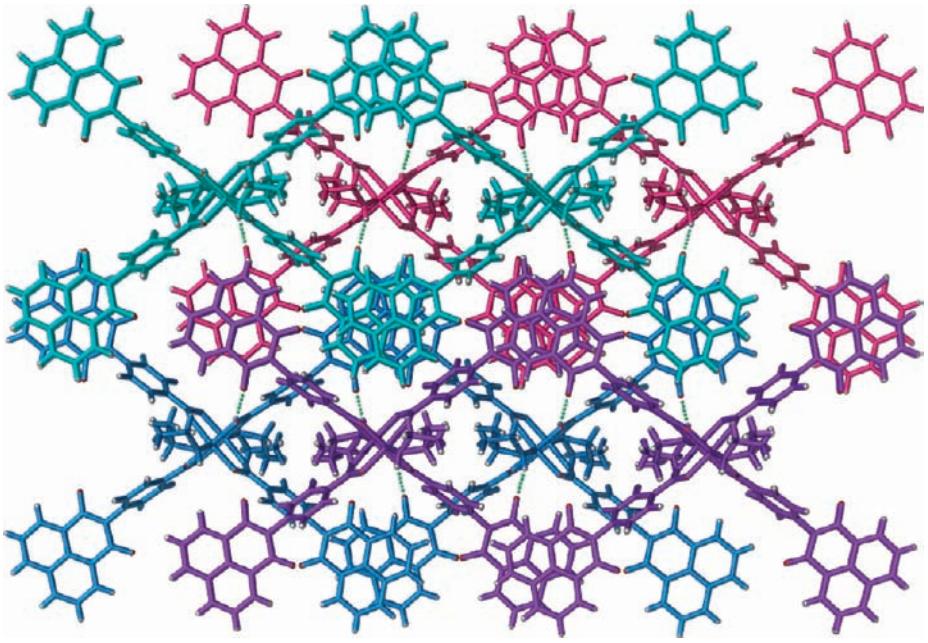

Figure 9. Two interpenetrated three-dimensional networks in the structure of **3.** The blue and purple colors delineate each network, the light and dark colors indicate six dimers within each network. The hydrogen bonding interactions between the two networks are indicated by the green dots.

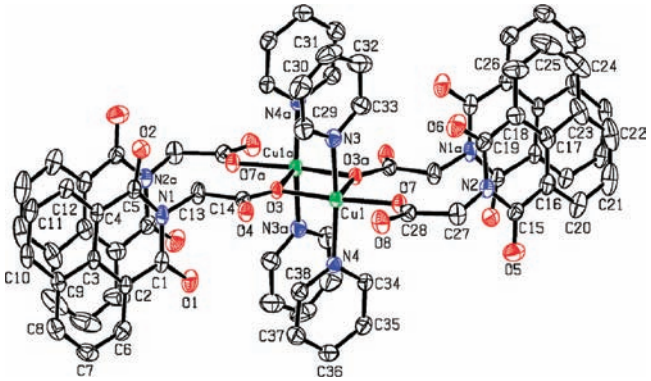

Figure 10. Molecular structure of $[Cu_2(L_{C1})_4(py)_4]\cdot 2(CH_2Cl_2)$ (**4**). Hydrogen atoms and some labels are omitted for clarity.

the pyridine rings links the two sheets together into a three-dimensional architecture.

Thermogravimetric Analysis. Thermogravimetric analysis was carried out on crystals of **3** and **4**. For **3** the TGA/DTA curves, Figure 14, show a four step thermal decomposition. The first step between 26 and 194 °C with a mass loss of 9.2% corresponds to the loss of two dichloromethane solvent molecules (calcd. 10.3%). The PXRD spectrum of the solid analyzed at this point (Supporting Information, Figure S5) indicates the sample retains crystallinity and the main features of the spectrum are matched by a calculated spectrum based on the single-crystal X-ray structure of **3** with the solvent removed. In the second step between 194 and 327 °C the loss of the two coordinated ethanol molecules occurs (4.4%, calcd: 5.6%). In the last two steps between 327 and 558 °C the four carboxylate ligands are lost and the framework decomposes (77.4%, calcd: 74.5%). The final residual weight is 9.0% corresponding to CuO (calcd. 9.6%).

In the case of **4** one dichloromethane molecule was lost after the crystals were collected from the mother liquor. This result is in accordance with the TGA/DTA profile of the compound. Upon heating the weight loss of 5.5% (calcd 5.5%) in the first step corresponds to the loss of the second dichloromethane molecule of crystallization. In the next step, between 120 and 212 °C, two of the coordinated pyridine molecules are lost (10.5%, calcd 10.2%). The weight change in the last two steps corresponds to the loss of the other two pyridine molecules and the four carboxylate ligands (74.0%, calcd: 73.9%). The final residual weight is 10.0% corresponding to CuO (calcd 10.2%).

Magnetic Properties. Exchange coupling in a binuclear copper system, which is described by the Heisenberg–Dirac-Van Vleck Hamiltonian (HDVV)

$$\hat{H} = -J\hat{S}_1\cdot\hat{S}_2 \tag{1}$$

gives rise to two states of the total spin operator $\hat{S} = \hat{S}_1 + \hat{S}_2$. In the copper carboxylates, the singlet state ($S = 0$) is the ground state, while the triplet state ($S = 1$) is located typically ~300 cm^{-1} above it. In the notation used in this paper, the energy difference $E_{S=1} - E_{S=0}$ equals $-J$. The magnetic susceptibility χ_d, related to one copper equals

$$\chi_d = \frac{Ng^2\mu_B^2}{3kT}\frac{3\exp(J/kT)}{1+3\exp(J/kT)} \tag{2}$$

The susceptibility should approach zero at the lowest temperatures, but dimeric complexes are almost always contaminated by small amounts of monomeric impurities. Assuming that the impurities obey the Curie law, the formula needed to fit magnetic susceptibility data becomes

$$\chi = (1-f)\chi_d + f\chi_{mono} \tag{3}$$

where

$$\chi_{mono} = (Ng^2{\mu_B}^2/3kT)\cdot 1/2\cdot(1/2+1) \tag{4}$$

and f is the fraction of copper ions bound in monomeric molecules.

Our complexes contain large amounts of loosely bound solvents in their crystal lattices that tend to be lost over time

dx.doi.org/10.1021/ic202198k | Inorg. Chem. 2012, 51, 1068–1083

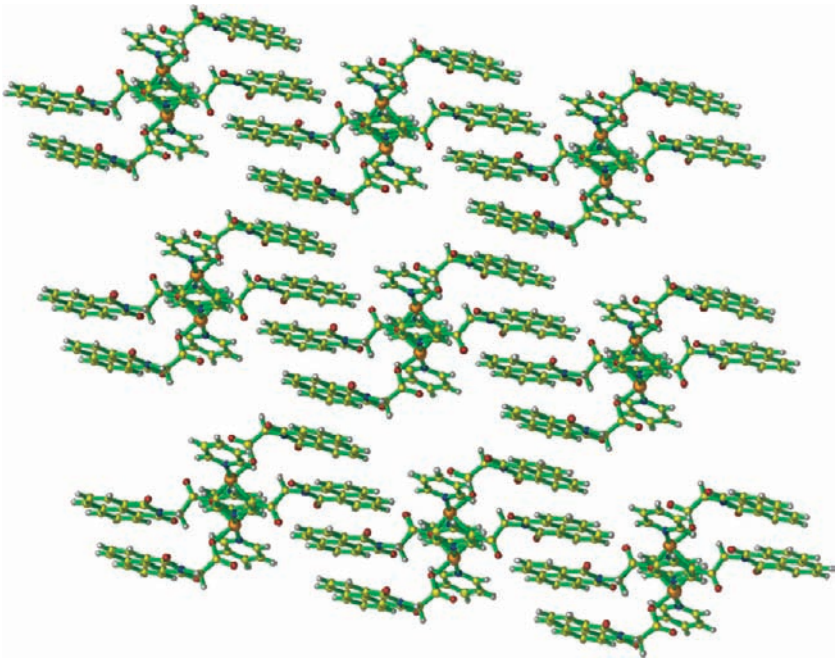

Figure 11. Sheet structure of **4**.

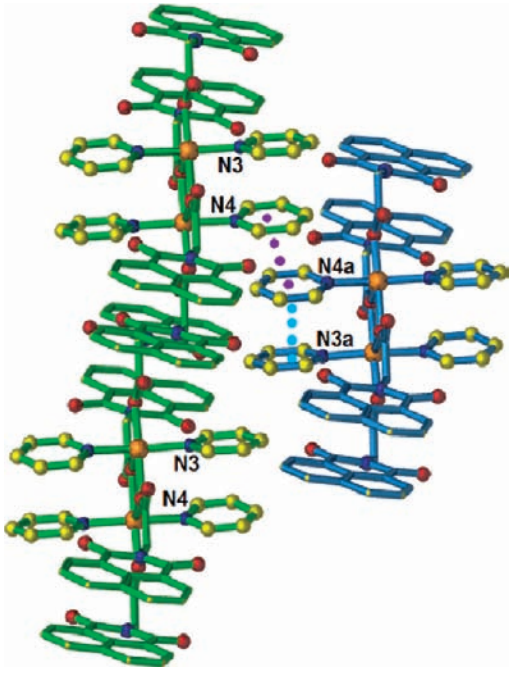

Figure 12. $\pi\cdots\pi$ stacking interactions (marked by the purple and light blue dots) of the coordinated pyridine molecules in the structure of **4**.

causing an uncertainty in the effective molar mass of a compound at the time of the magnetic susceptibility measurement. The molar mass appears as a multiplicative factor when converting the measured gram-susceptibility to the molar magnetic susceptibility. Using the full molar mass for that conversion after a partial solvent loss has occurred will cause the molar susceptibility to be too high, and the magnetic fitting will produce g values that are too large. In the present work advantage was taken of accurate knowledge of the g values from our high-field EPR experiments. The average g_{EPR} value obtained from EPR, $g_{EPR} = (g_x + g_y + g_z)/3$, was used together with the $g_{magnetic}$ value resulting from the magnetic susceptibility fitting to estimate the effective molar mass MM_{eff} by using the formula

$$MM_{eff} = (g_{EPR}/g_{magnetic})^2 \cdot MM_{X\text{-ray}} \quad (5)$$

This approach appears to have given sensible results.

As would be expected from the structures of **1**−**3**, all three complexes show substantial antiferromagnetic behavior, see Table 2. For completeness, we include in the table values for the complexes published in our previous work[9a,b] as well as some "typical" complexes from the literature. The temperature dependence of the molar magnetic susceptibility, χ_M, is shown in Figure 16 for complex **3** (see Supporting Information for complexes **1** and **2**). The magnetic fitting produced $J = -255$ cm^{-1}. This value and the values for the other complexes reported below, that range from −255 to −341 cm^{-1}, are rather typical.[10−13] The fraction of monomeric impurities was found to depend on the samples age, in agreement by visual detection of the crystal deterioration over time.

Complex **4** has a very different structure that provides no efficient path for exchange interactions. A very small antiferromagnetic J value of −1.7 cm^{-1} was determined, see Supporting Information Figure S3.

EPR Spectra. EPR spectra of the triplet states were interpreted in terms of the spin Hamiltonian

$$\hat{H} = \mu_B B\cdot\mathbf{g}\cdot\hat{S} + D\{\hat{S}_z^{\,2} - S(S+1)/3\} + E(\hat{S}_x^{\,2} - \hat{S}_y^{\,2}) \quad (6)$$

The spin Hamiltonian parameters are reported in Table 2 and representative spectra are shown in Figure 17 and in the Supporting Information. The values listed in Table 2 for complexes **5**−**8** are also new data, EPR spectra were not measured at the time of our previous publication.[9a] All seven of the paddlewheel complexes studied here exhibited remarkably axial EPR spectra (that is g_x was very close to g_y and the E parameter was very close to 0). It should be emphasized that no difference between g_x and g_y could be detected at microwave frequencies as high as 416 GHz for complexes **1**−**3** and **8** and

dx.doi.org/10.1021/ic202198k | Inorg. Chem. 2012, 51, 1068−1083

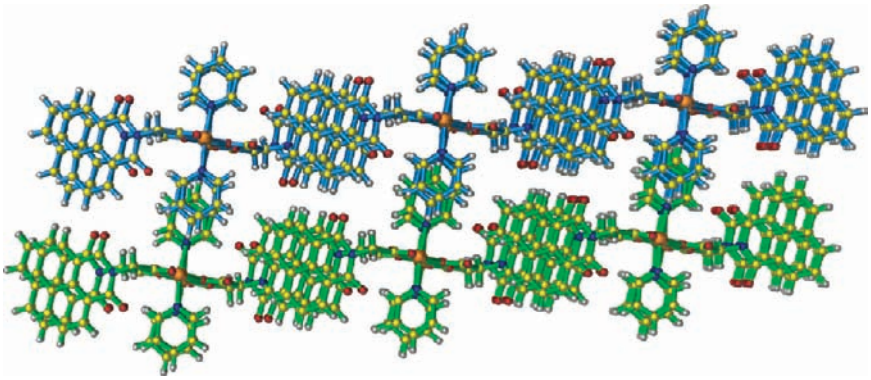

Figure 13. Three-dimensional structure of **4**. Two sheets are shown (blue and green bonds): the bottom sheet with green bonds is as pictured in Figure 12, but rotated by 90° in horizontal direction.

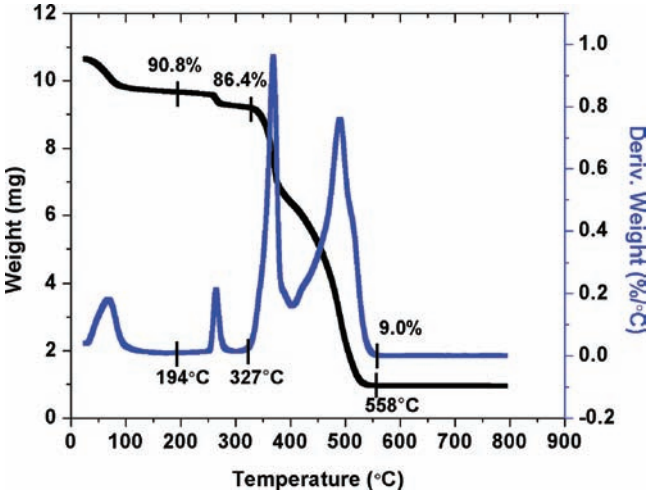

Figure 14. TGA-DTA curves for **3**..

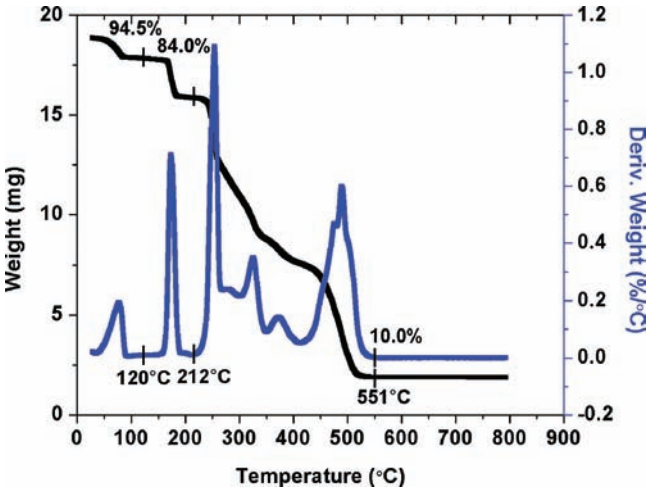

Figure 15. TGA-DTA curves for **4**.

the tiny differences observed in complexes **5**-**7** would not be detected in standard EPR. Large g components found here (g_z > 2.35 in each case) are characteristic for copper(II) in an oxygen coordination environment. No copper hyperfine structure could be observed, although other dimeric copper carboxylates sometimes exhibit it.[13d,e] The spin Hamiltonian parameters were only weakly temperature dependent (Table 2).

As shown in Figure 17, complex **1** exhibits resonance lines much broader than the other complexes in this series. The line width increases strongly with the microwave frequency indicating the "g-strain", distribution of g values which may be caused by disorder of some kind, likely involving the solvent. As also shown, complex **7**, $[Cu_2(\mathbf{L}_{C2})_4(bipy)]$, reported earlier shows a much larger zero-field splitting parameter D than any of the known copper "paddlewheel" dimers (see below).

The EPR spectra of complex **4**, Figure 18, were very different from the other complexes, showing very small zero-field splitting (zfs) parameters accompanied by g values lower than in the paddlewheel compounds, in accord with the replacement of two equatorial oxygen ligands by the nitrogen ligands. In this case, the simulation was rather imperfect compared to the paddlewheel complexes and the accuracy of the D determination is lower. The possible reasons are very small splitting, comparable to the line width at the "parallel" orientation and noncoaxiality of the g and zfs tensors. Weakening of the high-field "parallel" transition (right-hand part of the broad line at ca. 12.6 T) with decreasing temperature indicates a negative sign for D.

Calculation of the Exchange Integrals from DFT. We have attempted to calculate the exchange integrals at the DFT level by using the "broken symmetry" method.[20] In doing so, the simplified structures of the dimers were used in which all atoms were retained at their X-ray positions, but the long tails of the ligands were cut off. The ORCA calculation utilized Ahlrichs-type basis set TZVPP[21a] for copper and SVP[21] for other atoms, combined with the B3LYP[22] functional. Ahlrichs polarization functions from basis H − Kr R and auxiliary bases from the TurboMole library were also used.[21c] In the "broken symmetry" formalism applied for a copper dimer, one places 1 unpaired electron localized on site A and 1 unpaired electron localized on a site B and performs two separate spin-unrestricted SCF calculations: the first one is for the high-spin state with total spin equal to 1 and the second is a "broken symmetry" calculation with one spin-up orbital that is quasi-localized on site A and one spin-down orbital that is localized on site B.

Results obtained for complex **3** may be considered as representative for all paddlewheel complexes studied in this work, except for **7**. The orbital containing the unpaired electron for each is pictured in Figure 19. The calculation for **3** gave J = −383 and for **7** J = −350 cm^{-1} was obtained. For **3** the Mulliken population analysis (with ORCA) shows that the spin density is mainly in the $d_{x^2-y^2}$ orbital of Cu (0.70), with a small

dx.doi.org/10.1021/ic202198k | Inorg. Chem. 2012, 51, 1068−1083

Table 2. Solid State Magnetic and EPR Properties

complex		g_x	g_y	g_z	D, cm^{-1}	E, cm^{-1}	- J, cm^{-1}
1	284 K	2.067	2.067	2.360	−0.333[a]	0	310
	170 K	2.068	2.068	2.363	−0.333	0	
2	284 K	2.068	2.068	2.367	−0.347	0	325
	200 K	2.068	2.068	2.367	−0.347	0	
3	283 K	2.071	2.071	2.374	−0.341	0	255
	200 K	2.070	2.070	2.372	−0.339	0	
	120 K	2.069	2.069	2.371	−0.336	0	
	80 K	2.068	2.068	2.370	−0.336	0	
4	50 K	2.052	2.064	2.292	−0.033	0.005	1.7
5[g]	284 K	2.069	2.072	2.369	−0.349	0.0011	321
6[g]	300 K,	2.066	2.073	2.374	−0.360	0.0020	341
	200 K	2.066	2.066	2.374	−0.360	0.0020	
7[g]	300 K	2.077	2.089	2.350	−0.444	−0.0028	270
	283 K	2.079	2.090	2.352	−0.444	−0.0036	
	200 K	2.075	2.090	2.354	−0.460	−0.0059	
8[g]	300 K	2.071	2.071	2.364	−0.351	0	-[h]
	200 K	2.069	2.069	2.364	−0.351	0	
$[Cu(CH_3COO)_2H_2O]_2$	80 K[b]	2.054	2.079	2.364	−0.335	−0.0103	298[c]
$[Cu(CH_3COO)_2(pyr)]_2$	80 K[b]	2.061	2.062	2.349	−0.328	0	325[d]
$[Cu(CF_3COO)_2(quin)]_2$	80 K[e]	2.084	2.084	2.412	−0.433	0	310[f]

[a]Sign of D was assumed (see text). [b]EPR parameters from ref 13d. [c]Güdel, H. U.; Stebler, A.; Furrer, A. *Inorg. Chem.* **1979**, *18*, 1021. [d]Valentine, J. S.; Silverstein, A. J.; Soos, Z. G. *J. Am. Chem. Soc.* **1974**, *96*, 97. [e]EPR parameters from ref 13e. [f]Morosin, B.; Hughes, R. C.; Soos, Z. G. *Acta Cryst.* **1975**, *B31*, 762. [g]**5** = $[Cu_2(\mathbf{L}_{C2})_4(py)_2]\cdot 2(CH_2Cl_2)\cdot(CH_3OH)$, **6** = $[Cu_2(\mathbf{L}_{C3})_4(py)_2]\cdot 2(CH_2Cl_2)$, **7** = $[Cu_2(\mathbf{L}_{C2})_4(bipy)]$; **8** = $[Cu_2(\mathbf{L}_{C3})_4(bipy)]\cdot(CH_3OH)_2\cdot(CH_2Cl_2)_{3.37}$. [h]No value is reported for **8** because the polymorph that was studied by crystallography could not be reformed for a magnetic study.

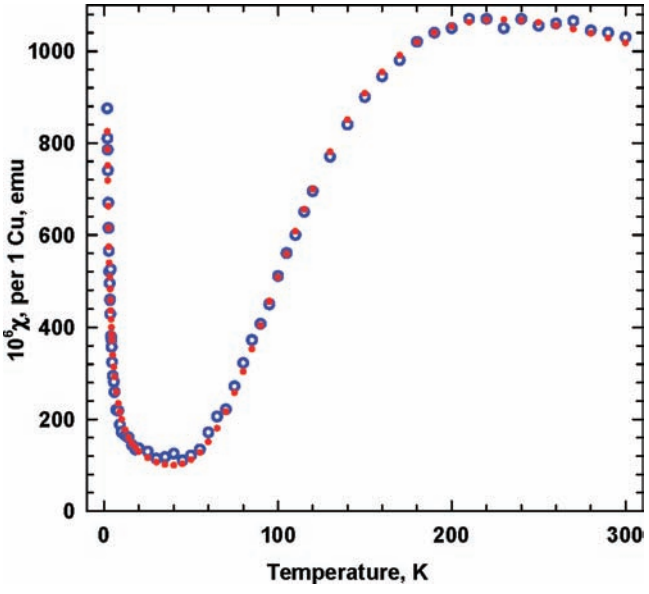

Figure 16. Temperature dependence of χ_M for complex **3**. Open circles: experimental. Dots: calculated with $J = -255$ cm^{-1}, $g = 2.21$, $f = 0.0033$. The average $g_{EPR} = 2.172$, hence the effective molar mass is 1598 (compared to 1654 from the crystal structure) indicating a partial solvent loss.

contribution of d_{z^2} (0.0066). The average spin density on the carboxylate oxygen atoms is 0.079 and no delocalization onto the axial alkoxo oxygen is observed. It is thus noteworthy that the unpaired electron density in **7** extends toward the axial nitrogen ligand (0.012), in contrast to other paddlewheels, while the carboxylate oxygen atoms contribution does not change much (0.074 on average). Also, the contribution of d_{z^2} is elevated to 0.043, while that of $d_{x^2-y^2}$ is slightly lowered down to 0.65. This altered electronic structure is likely causing the unusually large spin Hamiltonian parameter D in **7**. Contribution of d_{z^2} to the ground state in **7** should cause a decrease in g_z and an increase in g_x and g_y, which is indeed observed (Table 2). In both **3** and **7** the overlap integral of the unpaired electron orbitals (those shown in Figure 19) with their partners centered on the other copper is ~0.11 (from ORCA).

For complex **4**, in the exchange interaction pathways each bridging oxygen atom is an equatorial ligand of one copper(II) ion, but is an axial ligand of another copper(II) ion. In this arrangement, no strong antiferromagnetic interaction can be transmitted, because the interacting orbitals do not overlap sufficiently. Accordingly, the exchange integral of only −1.7 cm^{-1} was determined from the magnetic susceptibility data. The orbital of the unpaired electron of one copper(II) ion is shown in Figure 20, and the overlap integral with a corresponding orbital of the other copper(II) ion is 0.022. The "broken symmetry" calculation resulted in $J = -3.4$ cm^{-1}, in reasonable agreement with experiment.

The zero-field splitting (zfs) of the triplet state of copper dimers is caused by the combined effect of the magnetic dipole–dipole interactions and exchange coupling anisotropy.[13,23]

$$D = D_{exchange} + D_{dipole}, \quad E = E_{exchange} + E_{dipole} \qquad (7)$$

Although the dipole–dipole and anisotropic exchange contributions cannot be determined separately, the former one can be estimated from structures of binuclear systems.[10a,13,23] In the copper paddlewheel dimers the g_z direction is parallel to the Cu···Cu vector and D_{dipole} can be calculated from[10a,13]

$$D_{dipole} = -(2g_z^2 + (g_x^2 + g_y^2)/2)\mu_B^2/2r^3_{Cu—Cu} \qquad (8)$$

which results in D of about −0.18 cm^{-1} for a typical Cu···Cu distance of 2.64 Å, while E_{dipole} is close to zero. The point dipole model used above may be too crude an approximation as it takes no electron delocalization into account. In a recent

dx.doi.org/10.1021/ic202198k | *Inorg. Chem.* 2012, 51, 1068–1083

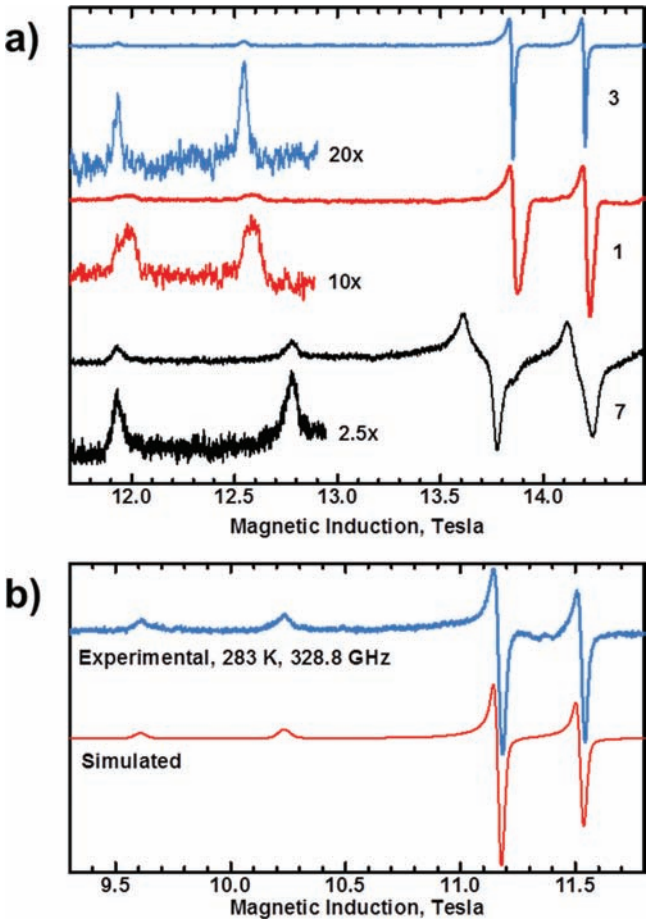

Figure 17. (a) High-field EPR spectra of **1**, **3**, and **7** recorded at 200 K with the microwave frequency 406.4 GHz. The "parallel" parts of the spectra are magnified as indicated. The splitting of ~6100 G between the two "parallel" lines in **1** and **3** is typical for the paddlewheel dimers, while in **7** it is 8500 Gauss; (b) EPR spectrum of **2** measured at 283 K with the microwave frequency 328.8 GHz (top) and its simulation with the spin Hamiltonian parameters given in Table 2 (bottom). Small signals between the "perpendicular" resonances at ~11.3–11.4 T are due to monomeric impurities.

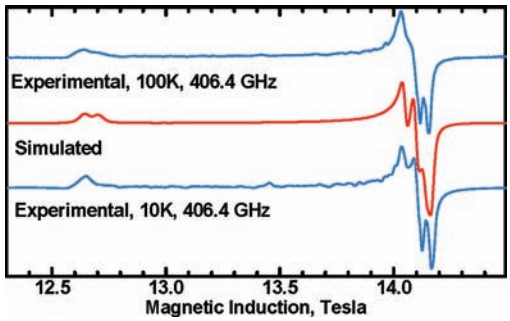

Figure 18. EPR spectra of complex **4** measured with the microwave frequency of 406.4 GHz at 100 K (top) and at 10 K (bottom). Central trace shows a simulation with $g_x = 2.052$, $g_y = 2.064$, $g_z = 2.292$, $D = -0.0327$ cm^{-1}, $E = -0.0047$ cm^{-1}, at 100 K. The false noise seen inside the spectrum, but not outside is caused by imperfect grinding of a very small sample.

paper[13f] it was shown by sophisticated DFT calculations that the actual D_{dipole} is around -0.12 cm^{-1}. In our paddlewheel complexes, the Cu···Cu distance varies between 2.61 and 2.69 Å resulting in D_{dipole} from the point-dipole model of -0.19 to -0.17 cm^{-1}.

In complex **4**, $r_{Cu\cdots Cu} = 3.38$ Å and $D_{dipole} = -0.078$ cm^{-1}, while the experimental D parameter is only -0.038 cm^{-1}. The discrepancy may be caused by electron delocalization and the anisotropic exchange contribution.

The anisotropic exchange component of zfs, $D_{exchange}$, is related to the exchange interactions in excited states of a dimeric molecule.[10a,13,23] In these excited states, the unpaired electron of one copper(II) ion is in one of the excited orbitals d_{xy}, d_{xz}, d_{yz}, while the other copper(II) ion is still in the ground state $d_{x^2-y^2}$. The exchange contribution to D is[10a,13,23]

$$D_{exchange} = -[J(x^2 - y^2, xy)\Delta_z^2 - 2J(x^2 - y^2, xz)\Delta_y^2 - 2J(x^2 - y^2, yz)\Delta_x^2]/32 \quad (9)$$

where $\Delta_z = g_z - 2.0023$, etc., and the first term in bracket is expected to be dominant. $J(x^2 - y^2,n)$ represent the triplet-singlet separations in the excited dimer states defined above. A different formula using no Δ_i quantities has been derived recently (eq 14 in ref 13f)

To extract the anisotropic exchange contribution to zfs, D_{ex}, one has to determine the experimental D parameter and subtract the calculated dipole–dipole part. Hence, knowledge of the sign of D is crucial for D_{ex} determination. The negative sign of D in paddlewheel complexes was determined from high-frequency EPR[13d,e] and was recently confirmed by theoretical calculations.[13f] The experimental D values of all paddlewheels presented in Table 2, including simple copper acetate, but excluding **7** and the copper trifluoroacetate complex, span a very narrow range of -0.33 to -0.36 cm^{-1}. The anisotropic exchange contribution is thus about -0.16 cm^{-1} when using D_{dipole} from eq 8, or about -0.21 cm^{-1} with D_{dipole} of -0.12 cm^{-1} according to ref 13f. The exchange contribution in **7** of about -0.27 cm^{-1} to -0.32 cm^{-1}, is even larger than in copper trifluoroacetate dimer. Large D parameters in copper paddlewheels formed by halogenated aliphatic acids,[12] like trifluoroacetic,[13e] are accompanied by strongly elevated g values (Table 2) and can be interpreted as a result of a reduced unpaired electron delocalization onto the carboxylate oxygen atoms (i.e., less covalent bonds). This is clearly not the case in **7**, where the g values are not elevated. The increased exchange contribution to D in **7** must be correlated to the specific structure of this complex. In contrast to other compounds in this series, **7** is distorted toward a compressed trigonal-bipyramid whose base is formed by atoms N3, O4 and O8. The bipyramid axes of two copper(II) ions are roughly perpendicular to each other and the dimer molecule has no inversion center. The magnetic orbitals of each copper ion in **7** contain a contribution of d_{z^2}, while pure $d_{x^2-y^2}$ is found for other paddlewheels (see Figure 19).

With a d_{z2} contribution to the ground state, formula 9 above will depend on additional exchange interactions in the excited states. Considering the nonzero matrix elements of the operators $\mathbf{L}_x$, $\mathbf{L}_y$ and $\mathbf{L}_z$ between d_{z^2} and other d orbitals, the exchange interactions $J(z^2, xz)$, $J(z^2, yz)$ should be taken into account in a corrected eq 9. While it appears understandable that the zfs should be affected, not even a qualitative prediction concerning the direction or magnitude of the resulting change in D appears to be possible. The information of the exchange interactions in excited states of a dimer is extremely difficult to obtain experimentally[23] or from theory.[13f]

dx.doi.org/10.1021/ic202198k | Inorg. Chem. 2012, 51, 1068–1083

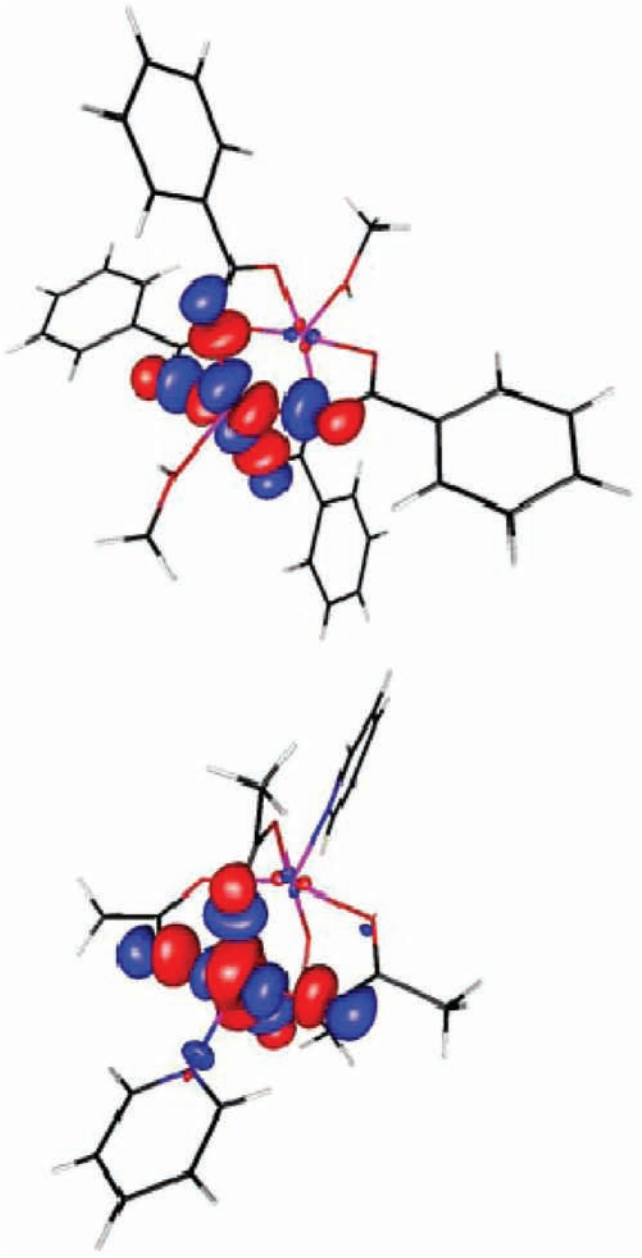

Figure 19. Unpaired electron orbitals for **3** (top) and **7** (bottom) resulting from the "broken symmetry" calculations. Orbitals of identical shape localized on the opposite copper atoms are not plotted for clarity. In **7**, the unpaired electron appears to be engaged in a σ bond to an axial nitrogen ligand, while in **3** and other paddlewheels no unpaired electron delocalization toward the axial ligands is observed. Bipy in **7** was shortened to pyridine and the acid was shortened to acetic. In **3**, the acid was shortened to benzoic to make the molecules manageable.

Another interesting aspect is that in a dimer with no inversion center, the antisymmetric exchange (Dzialoshinkii-Moriya interaction)[24] may contribute to zfs. However, the DM interaction does not seem to be essential here, given the fact that the EPR line positions of **7** are still correctly reproduced by using spin Hamiltonian (6).

DISCUSSION

Three new SMOF architectures assembled from the $Cu_2(O_2CR)_4$ SBU core, built from bifunctional carboxylate ligands bearing the 1,8-naphthalimide group that form a robust π-stacking supramolecular synthon and all bearing hydrogen bonding axial ligands, were prepared and structurally analyzed. The molecular and supramolecular structure of **1** is similar to the $[Cu_2(\mathbf{L_{C2}})_4(py)_2]\cdot 2(CH_2Cl_2)\cdot(CH_3OH)$ (**5**) complex of this same ligand discussed in our previous work.[9a] As anticipated from the design of the system, in both compounds the SBU cores are linked by the $\pi\cdots\pi$ stacking of the naphthalimide rings into a two-dimensional sheet structure. The arms of the $\mathbf{L_{C2}}^-$ ligand are fairly coplanar and directed in the four directions imposed by the SBU core. While the two-dimensional sheet structure of the two compounds is held together by the same type of forces, there are important differences in the three-dimensional architecture of these complexes due to the introduction of the methanol axial ligands in **1**, ligands that can enter into hydrogen bonding interactions. In the case of **5**, the third direction is supported only by $\pi\cdots\pi$ stacking of the naphthalimide rings. For **1**, this direction is also supported by $\pi\cdots\pi$ stacking, but in addition there are hydrogen bonding interactions of the methanol axial ligands, interactions that shorten the distance between the dimeric units (5.19 vs 8.51 Å).

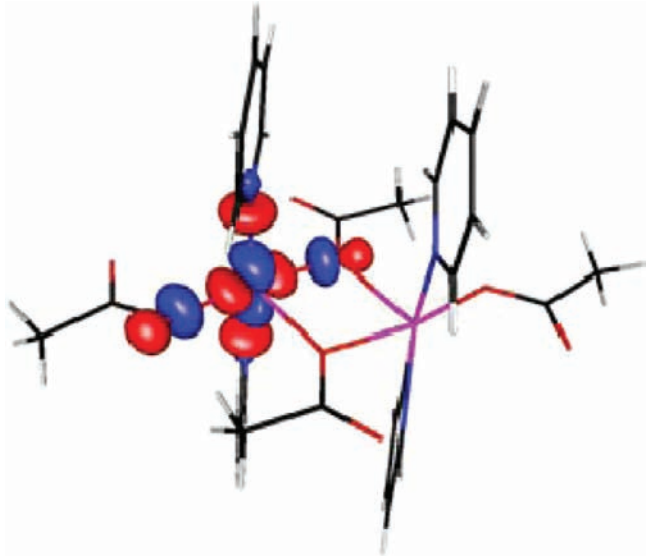

Figure 20. Unpaired electron orbital in **4**, illustrating an inefficient exchange pathway through the oxygen ligands.

Shortening the link between the two functional groups to a single CH_2 group in the $\mathbf{L_{C1}}^-$ ligand causes changes in the orientation of the naphthalimide rings in **2** away from the "square" architecture of the SBU core and directs them at an angle of 114°. In the structure, two sets of adjacent naphthalimide groups are oriented above and below the plane of the square SBU unit. Despite the difference in the orientation of the naphthalimide rings with respect to the dimeric SBU cores when compared with **1**, again all four naphthalimide rings of the dimeric units are involved in $\pi\cdots\pi$ stacking that forms an overall structure of a two-dimensional sheet held together by noncovalent forces. Additionally, in both cases the methanol molecules bounded to the axial positions enter into hydrogen bonding interactions generating a three-dimensional architecture. The differences arise in the noncovalent forces that support the third dimension in the two solids. While in **1** the orientation of the naphthalimide rings allows additional strong $\pi\cdots\pi$ stacking interactions in the third

dx.doi.org/10.1021/ic202198k | Inorg. Chem. 2012, 51, 1068–1083

Table 3. Important Metric Parameters for Paddlewheel Compounds 1−3 and 5−8

compound	Cu···Cu (Å)	Cu−O (basal) (Å)	Cu−L (axial) (Å)	O−C (Å)	Cu−O−C (deg)	O−C−O (deg)	Cu−O−C−O−Cu (Å)	τ
$[Cu_2(L_{C2})_4(CH_3OH)_2]$ (**1**)	2.6080(8)	1.961	2.166(3)	1.261	122.42	125.75	6.44	0.004
$[Cu_2(L_{C1})_4(CH_3OH)_2]\cdot(CH_2Cl_2)_2$ (**2**)	2.6287(8)	1.9625	2.157(3)	1.254	122.18	126.8	6.43	0.004
$[Cu_2(L_{C4})_4(CH_3CH_2OH)_2]\cdot(CH_2Cl_2)_2$ (**3**)	2.6424(8)	1.967	2.157(3)	1.261	122.3	125.95	6.45	0.004
$[Cu_2(L_{C2})_4(py)_2]\cdot(CH_2Cl_2)_2\cdot(CH_3OH)$ (**5**)	2.6572(6)	1.9691	2.164(2)	1.258	123.06	125.55	6.46	0.010
$[Cu_2(L_{C3})_4(py)_2]\cdot(CH_2Cl_2)_2$ (**6**)	2.6632(5)	1.9718	2.1796(18)	1.258	123.65	125.15	6.46	0.001
$[Cu_2(L_{C2})_4(4,4'\text{-bipy})]$ (**7**)	2.6870(9)	1.9808	2.120(3)	1.257	123.28	125.1	6.48	0.29
$[Cu_2(L_{C3})_4(4,4'\text{-bipy})]\cdot(CH_2Cl_2)_{3.37}(CH_3OH)_2$ (**8**)	2.6147(8)	1.9725	2.150(3)	1.257	123	124.9	6.46	0.005

dimension, the different orientation in **2** allows only hydrogen bonding of the coordinated methanol molecules. The different orientation of the naphthalimide groups with respect to the SBU core, forced by the change from a C2 to a C1 linker in the ligand, does not allow $\pi\cdots\pi$ stacking between the sheets in **2**. This difference in structure brings out an important issue for the 1,8-naphthalimide supramolecular synthon − in structures as observed for complex **1** strong $\pi\cdots\pi$ stacking interactions can form on *both sides of the ring* making it a versatile building block for three-dimensional SMOFs. By changing the design of the ligand in **2**, this "two-sided" interaction is prevented.

The L_{C4}^- ligand, which has a long, linear link between the two functional groups, was designed to prepare structures that would retain the "square" architecture of the SBU core, but also produce open structures. Its dicopper complex has a unique 2-fold interpenetrated three-dimensional architecture. As shown in Figure 8, the linear directional orientation of the phenylene arms places the naphthalimide rings of the SBUs in positions in which the dipole vectors of the rings from adjacent dimeric units can form $\pi\cdots\pi$ stacking interactions at nearly right angles, leading to the formation of a three-dimensional open framework. The accessible region in this open network is occupied by interpenetration of a second three-dimensional network structure (Figure 9) and the two dichloromethane solvent of crystallization.

Surprisingly, the reaction of the L_{C1}^- ligand with $Cu_2(O_2CCH_3)_4(H_2O)_2$ in the presence of pyridine yields a very different type of dimeric tetracarboxylato copper compound, **4**, when the reaction is carried out at −20 °C when compared to compound **2**, which forms at room temperature. Compound **4** has an unusual dimeric structure containing two $\mu-\kappa^1$-carboxylate ligands rather than the paddlewheel structure of **1**−**3**. A consequence of this new dimeric arrangement is that adjacent naphthalimide rings are oriented in close proximity so as to form the only example of intramolecular $\pi\cdots\pi$ stacking in the copper(II) complexes of this family of ligands.[9] The intermolecular $\pi\cdots\pi$ stacking of the naphthalimide rings generates the anticipated sheet structure, but in contrast to our earlier structures with axial pyridine ligands in paddlewheel complexes,[9a] $\pi\cdots\pi$ stacking of the pyridine rings links the sheets in the third dimension.

We have shown that judicious ligand design can lead to novel SMOF materials in which the building units are held together by a combination of covalent and noncovalent forces. A particularly attractive feature of these bifunctional ligands that can form the 1,8-naphthalimide supramolecular synthon is the ease of ligand synthesis in a one pot condensation reaction from commercially available amino acids and naphthalic anhydride. The new paddlewheel dicopper tetracarboxylato complexes (**1**−**3**) discussed in this paper, along with the four compounds in our original study, demonstrate that the 1,8-naphthalimide groups enter into strong $\pi\cdots\pi$ stacking interactions, interactions that can be transferred from one system to another to generate high-dimensionality materials. In the structures reported here, we demonstrate that the introduction of axial ligands that can enter into hydrogen bonding interactions can add to the organization of the SMOF solid. Although these solids are not a robust as classical MOFs, the TGA studies do demonstrate that they are robust materials.

Moreover, the ease of structural variation of the bifunctional ligands (by controlling the type of link between the carboxylate donor group and naphthalimide rings) allows us to modify the way SBUs are assembled into a desired superstructure. The short L_{C1}^- ligand incorporated into a copper(II) paddlewheel system will promote the formation of a two-dimensional sheet, the single CH_2 linker does not allow $\pi\cdots\pi$ stacking between the sheets. With this ligand, the extension of the structure into the third dimension can be achieved only by the presence of an axial ligand capable of hydrogen-bonding (or some other) interactions. The semirigid L_{C2}^- ligand, however, allows the formation of a fully three-dimensional architecture assembled only by the $\pi\cdots\pi$ stacking interaction of the naphthalimide rings. More open three-dimensional structures can be produced by the rigid L_{C4}^- ligand, which has a long, linear link between the two functional groups. The accessible region in this framework can possibly be occupied by interpenetration of a second three-dimensional network to generate a 2-fold interpenetrated three-dimensional architecture.

Additionally, incorporating the $Cu_2(O_2CR)_4$ unit into highly organized solids can lead to three-dimensional materials with interesting magnetic and EPR properties. In the four compounds reported in our previous study and the three paddlewheel compound reported here, the copper centers are strongly antiferromagnetically coupled with $-J$ values ranging from 255 to 341. Extensive work has been dedicated to study the strong antiferromagnetic coupling in paddlewheel dicopper-tetracarboxylates. It is believed that in these systems, the unpaired electrons of the d^9 copper(II) ions are coupled through the carboxylate bridges, an interaction known as superexchange that leads to a singlet ground state.[10,13] The magnitude of this intramolecular exchange interaction, J, is equal to the singlet−triplet energy separation, and is thought to be influenced by several factors, such as the stereochemistry of the copper(II) ions, the bond angles at bridging atoms, and the copper-bridge ligand bond lengths. Table 3 contains a comparison of relevant structural parameters of **1**−**3** and the four dicopper tetracarboxylato compounds from our previous study. No obvious trends emerge from these data to explain the trends in J. The one factor that does stand out from Table 3, although it does not seem to impact on the J values, is the

dx.doi.org/10.1021/ic202198k | Inorg. Chem. 2012, 51, 1068−1083

difference for complex **7** in the Addison τ factor, a parameter that describes the distortion from the square pyramidal to trigonal bipyramidal geometry,[25] where for a square pyramid $\tau = 0$ and for a trigonal-bipyramid $\tau = 1$. We also note that as expected from the large distances that separate dicopper cores in these complexes, the supramolecular structure does also not appear to influence the magnetic properties.

In general, the spin Hamiltonian parameters *g*, *D* and *E* were similar to those reported earlier for copper(II) acetate axially coordinated by organic molecules, with the notable exception of **7**, which showed *D* even larger than previously found for trifluoroacetate paddlewheels (Table 2). The DFT results indicate that the large *D* value for **7** likely to be a result of the d_{z^2} orbital contribution to the ground state of copper(II) in this complex, forced out by the specific geometry of the copper coordination sphere. This difference in geometry is brought out by the large τ value for **7**, as shown in Table 3.

■ ASSOCIATED CONTENT

Ⓢ Supporting Information

X-ray crystallographic files in CIF format for the structural determinations, detailed description of the X-ray structural analysis, table of bond lengths and angles, magnetic plots for complexes **1**, **2**, and **4**, X-Band EPR spectra of **1** and **7**, and PXRD data for desolvated **3**. This information is available free of charge via the Internet at http://pubs.acs.org.

■ AUTHOR INFORMATION

Corresponding Author

*Email: reger@mail.chem.sc.edu (D.L.R.); ozarowsk@magnet.fsu.edu (A.O.).

■ ACKNOWLEDGMENTS

The authors (DLR) acknowledge with thanks the financial support of the National Science Foundation through grant CHE-1011736. The high-field EPR spectra were recorded at the NHMFL, which is funded by the NSF through the Cooperative Agreement No. DMR-0654118, the State of Florida and the DOE. The magnetic measurements were supported by the Polish Ministry of Science and Higher Education through Grant No. N N204 013936. We thank Professors Gary J. Long, Missouri University of Science and Technology, and Fernande Grandjean, University of Liège, for helpful discussions of the magnetic data and Dr. Daniel E. Bugaris for running the powder XRD.

■ REFERENCES

(1) (a) Phan, A.; Czaja, A. U.; Gandara, F.; Knobler, C. B.; Yaghi, O. M. *Inorg. Chem.* **2011**, *50*, 7388. (b) Dhakshinamoorthy, A.; Alvaro, M.; Corma, A.; García, H. *Dalton Trans.* **2011**, *40*, 6344. (c) Corma, A.; García, H.; Llabrés i Xamena, F. X. *Chem. Rev.* **2010**, *110*, 4606 and references therein. (d) Farrusseng, D.; Aguado, S.; Pinel, C. *Angew. Chem., Int. Ed.* **2009**, *48*, 7502. (e) Tanabe, K. K.; Cohen, S. M. *Inorg. Chem.* **2010**, *49*, 6766. (f) Lin, W. *Top. Catal.* **2010**, *53*, 869. (g) Wu, C.-D.; Hu, A.; Zhang, L.; Lin, W. *J. Am. Chem. Soc.* **2005**, *127*, 8941. (h) Qiu, S.; Zhu, G. *Coord. Chem. Rev.* **2009**, *253*, 2891.

(2) (a) Zhao, D; Timmons, D. J.; Yuan, D.; Zhou, H.-C. *Acc. Chem. Res.* **2011**, *44*, 123. (b) Murray, L. J.; Dinca, M.; Long, J. R. *Chem. Soc. Rev.* **2009**, *38*, 1294. (c) Czaja, A. U.; Trukhan, N.; Muller, U. *Chem. Soc. Rev.* **2009**, *38*, 1284. (d) Muller, U.; Schubert, M.; Teich, F.; Puetter, H.; Schierle-Arndt, K.; Pastre, J. *J. Mater. Chem.* **2006**, *38*, 626. (e) Rowsell, J. C. L.; Spencer, E. C.; Eckert, J.; Howard, J. K.; Yaghi, O. M. *Science* **2005**, *309*, 1350. (f) Morris, R. E.; Wheatley, P. S. *Angew. Chem., Int. Ed.* **2008**, *47*, 4966. (g) Rowsell, J. L. C.; Yaghi, O. M. *Angew. Chem., Int. Ed.* **2005**, *44*, 4670. (h) Matsuda, R; Kitaura, R; Kitagawa, S; Kubota, Y; Belosludov, R. V.; Kobayashi, T. C.; Sakamoto, H.; Chiba, T.; Takata, M.; Kawazoe, Y.; Mita, Y. *Nature* **2005**, *436*, 238. (i) Millward, A. R.; Yaghi, O. M. *J. Am. Chem. Soc.* **2005**, *127*, 17998. (j) Ro, J. C.; Eckert, J.; Yaghi, O. M. *J. Am. Chem. Soc.* **2005**, *127*, 14904. (k) Li, Y.; Yang, R. T. *Langmuir* **2007**, *23*, 12937.

(3) (a) Chen, B.; Xiang, S.; Qian, G. *Acc. Chem. Res.* **2010**, *43*, 1115. (b) Liu, S.; Li, J.; Luo, F. *Inorg. Chem. Commun.* **2010**, *13*, 870. (c) Green, M. A. *Nat. Mater.* **2010**, *9*, 539. (d) Lan, A.; Li, K.; Wu, H.; Olson, D.; Emge, T.; Ki, W.; Hong, M.; Li, J. *Angew. Chem., Int. Ed.* **2009**, *48*, 2334. (e) Chen, B.; Yang, Y.; Zapata, F.; Lin, G.; Qian, G.; Lobkovsky, E. B. *Adv. Mater.* **2007**, *19*, 1693.

(4) (a) Basu, S.; Cano-Odena, A.; Vankelecom, I. F. J. *Sep. Purif. Technol.* **2011**, *81*, 31. (b) Czaja, A. U.; Trukhan, N.; Muller, U. *Chem. Soc. Rev.* **2009**, *38*, 1284 and references therein. (c) Qiu, S.; Zhu, G. *Coord. Chem. Rev.* **2009**, *253*, 2891. (d) Manos, M. J.; Iyer, R. G.; Quarez, E.; Liao, J. H.; Kanatzidis, M. G. *Angew. Chem., Intl. Ed.* **2005**, *44*, 3552. (e) Lee, H.; Zones, S. I.; Davis, M. E. *Nature* **2003**, *425*, 385. (f) Corma, A. *Chem. Rev.* **1997**, *97*, 2373 and references therein.

(5) (a) Zhao, L.-M.; Zhang, Z.-J.; Zhang, S.-Y.; Cui, P.; Shi, W.; Zhao, B.; Cheng, P.; Liao, D.-Z.; Yan, S.-P. *CrystEngComm.* **2011**, *13*, 907. (b) Tranchemontagne, D. J.; Mendoza-Cortes, J. L.; O'Keeffe, M.; Yaghi, O. M. *Chem. Soc. Rev.* **2009**, *38*, 1257. (c) Rao, C. N. R.; Natarajan, S.; Vaidhyanathan, R. *Angew. Chem., Int. Ed.* **2004**, *43*, 1466. (d) Yaghi, O. M.; O'Keeffe, M.; Ockwig, N. W.; Chae, H. K.; Eddaoudi, M.; Kim, J. *Nature* **2003**, *423*, 705. (e) Rosi, N. L.; Eddaoudi, M.; Kim, J.; O'Keeffe, M.; Yaghi, O. M. *CrystEngComm.* **2002**, *4*, 401. (f) Eddaoudi, M.; Moler, D. B.; Li, H.; Chen, B.; Reineke, T. M.; O'Keeffe, M.; Yaghi, O. M. *Acc. Chem. Res.* **2001**, *34*, 319.

(6) (a) Braga, D.; Maini, L.; Polito, M.; Tagliavini, E.; Grepioni, F. *Coord. Chem. Rev.* **2003**, *53*, 246. (b) Desiraju, G. R. *Acc. Chem. Res.* **2002**, *35*, 565. (c) Moulton, B.; Zaworotko, M. J. *Chem. Rev.* **2001**, *101*, 1629. (d) Desiraju, G. R. *J. Chem. Soc., Dalton Trans.* **2000**, 3745. (e) Braga, D.; Grepioni, F. *Acc. Chem. Res.* **2000**, *33*, 601. (f) Beatty, A. M. *Coord. Chem. Rev.* **2003**, *246*, 131. (g) Brammer, L. *Chem. Soc. Rev.* **2004**, *33*, 476.

(7) (a) Janiak, C. *J. Chem. Soc., Dalton Trans.* **2000**, 3885. (b) Hunter, C. A.; Sanders, J. K. M. *J. Am. Chem. Soc.* **1990**, *112*, 5525. (c) Steed, J. W.; Atwood, J. L. *Supramolecular Chemistry*, 2nd ed.; John Wiley&Sons, Ltd.: U.K., 2009; pp 33−35. (d) Amabilino, D. B.; Stoddart, F. J. *Chem. Rev.* **1995**, *95*, 2725. (e) Liu, Y.; Flood, A. H.; Bonvallet, P. A.; Vignon, S. A.; Northrop, B. H.; Tseng, H.-R.; Jeppesen, J. O.; Huang, T. J.; Brough, B.; Baller, M.; Magonov, S.; Solares, S. D.; Goddard, W. A.; Ho, C.-M.; Stoddart, J. F. *J. Am. Chem. Soc.* **2005**, *127*, 9745.

(8) (a) Reger, D. L.; Elgin, J. D.; Semeniuc, R. F.; Pellechia, P. J.; Smith, M. D. *Chem. Commun.* **2005**, 4068. (b) Reger, D. L.; Semeniuc, R. F.; Elgin, J. D.; Rassolov, V.; Smith, M. D. *Cryst. Growth Des.* **2006**, *6*, 2758. (c) Reger, D. L.; Elgin, J. D.; Smith, M. D; Simpson, B. K. *Polyhedron* **2009**, *28*, 1469.

(9) (a) Reger, D. L.; Debreczeni, A.; Reinecke, B.; Rassolov, V.; Smith, M. D.; Semeniuc, R. F. *Inorg. Chem.* **2009**, *48*, 8911. (b) Reger, D. L.; Horger, J. J.; Debreczeni, A.; Smith, M. D. *Inorg. Chem.* **2011**, *50*, 4669. (c) Reger, D. L.; Debreczeni, A.; Smith, M. D. *Inorg. Chim. Acta* **2010**, *364*, 10. (c) Reger, D. L.; Horger, J.; Smith, M. D. *Chem. Commun.* **2011**, *47*, 2805.

(10) (a) Bleaney, B.; Bowers, K. D. *Proc. Roy. Soc. London, A* **1952**, *214*, 451. (b) Cotton, F. A.; Wilkinson, G; Murillo, C. A.; Bochmann, M. *Advanced Inorganic Chemistry*; John Wiley & Sons, Inc.: New York, U.S.A., 1999; pp 870−871 (c) Kahn, O. *Molecular Magnetism*; VCH Publishers, Inc.: New York, U.S.A., 1993.

(11) Hay, P. J.; Thibeault, J. C.; Hoffmann, R. *J. Am. Chem. Soc.* **1975**, *97*, 4884.

(12) Melnik, M. *Coord. Chem. Rev.* **1981**, *36*, 1.

(13) (a) Abragam, A.; Bleaney, B. In *Electron Paramagnetic Resonance of Transition Ions*; Dover Publications, Inc.: New York, 1986. (b) Bencini, A.; Gatteschi, D. In *EPR of Exchange Coupled Systems*;

Springer Verlag: Berlin-Heidelberg, Germany, 1990. (c) Gribnau, M. C. M.; Keijzers, C. P. *Inorg. Chem.* **1987**, *26*, 3413. (d) Ozarowski, A. *Inorg. Chem.* **2008**, *47*, 9760. (e) Ozarowski, A.; Szymanska, I. B.; Muziol, T.; Jezierska, J. *J. Am. Chem. Soc.* **2009**, *131*, 10279. (f) Maurice, R.; Sivalingam, K.; Ganyushin, D.; Guihery, N.; de Graaf, C.; Neese, F. *Inorg. Chem.* **2011**, *50*, 6229.

(14) Reger, D. L.; Debreczeni, A.; Horger, J. J.; Smith, M. D. *Cryst. Growth Des.* **2011**, *11*, 4068.

(15) (a) O'Connor, C. J. *Prog. Inorg. Chem.* **1982**, *29*, 203. (b) Bain, G. A.; Berry, J. F. *J. Chem. Educ.* **2008**, *85*, 532.

(16) Hassan, A. K.; Pardi, L. A.; Krzystek, J.; Sienkiewicz, A.; Goy, P.; Rohrer, M.; Brunel, L.-C. *J. Magn. Reson.* **2000**, *142*, 300.

(17) *SMART*, version 5.630; *SAINT+*, version 6.45; *SADABS*, version 2.05; Bruker Analytical X-ray Systems, Inc.: Madison, Wisconsin, U.S.A., 2003.

(18) (a) Sheldrick, G. M. *SHELXTL*, version 6.14; Bruker Analytical X-ray Systems, Inc.: Madison, Wisconsin, U.S.A., 2000. (b) *CELL_NOW*; Bruker AXS Inc.: Madison, Wisconsin, U.S.A., 2005.

(19) (a) Castineiras, A.; Balboa, S.; Bermejo, E.; Carballo, R.; Covelo, B.; Borras, J.; Real, J. A. *Z. Anorg. Allg. Chem.* **2002**, *628*, 1116. (b) Christou, G.; Perlepes, S. P.; Libby, E.; Folting, K.; Huffman, J. C.; Webb, R. J.; Hendrickson, D. N. *Inorg. Chem.* **1990**, *29*, 3657. (c) Christou, G.; Perlepes, S. P.; Libby, E.; Folting, K.; Huffman, J. C.; Webb, R. J.; Hendrickson, D. N. *J. Chem. Soc., Chem. Commun.* **1990**, 746.

(20) Neese, F. *ORCA—An Ab Initio Density Functional and Semiempirical Program Package*, version 2.8; Universität Bonn: Bonn, Germany, 2008; free download from http://www.thch.uni-bonn.de/tc/orca/, registration required.

(21) (a) Schaefer, A.; Horn, H.; Ahlrichs, R. *J. Chem. Phys.* **1992**, *97*, 2571. (b) Ahlrichs, R. et al. Unpublished. (c) The Ahlrichs auxiliary basis sets were obtained from the TurboMole basis set library under ftp.chemie.uni-karlsruhe.de/pub/jbasen. (d) Eichkorn, K.; Treutler, O.; Ohm, H.; Haser, M.; Ahlrichs, R. *Chem. Phys. Lett.* **1995**, *240*, 283. (e) Eichkorn, K.; Weigend, F.; Treutler, O.; Ahlrichs, R. *Theor. Chem. Acc.* **1997**, *97*, 119.

(22) (a) Becke, D. A. *Phys. Rev. A* **1988**, *38*, 3098. (b) Perdew, J. P. *Phys. Rev. B* **1986**, *33*, 8822. (c) Perdew, J. P. *Phys. Rev. B.* **1986**, *34*, 7406. (c) Kendall, R. A.; Früchtl, H. A. *Theor. Chem. Acc.* **1997**, *97*, 158.

(23) Ross, P. K.; Allendorf, M. D.; Solomon, E. I. *J. Am. Chem. Soc.* **1989**, *111*, 4009.

(24) (a) Moriya, T. *Phys. Rev.* **1960**, *120*, 91. (b) Buckingham, A. D.; Pyykko, P.; Robert, J. B.; Wiesenfeld, L. *Mol. Phys.* **1982**, *46*, 177. (c) Lines, M. E.; Ginsberg, A. P.; Martin, R. L. *Phys. Rev. Lett.* **1972**, *28*, 684.

(25) (a) Addison, A. W.; Rao, N. T.; Reedijk, J.; van Rijn, J.; Verschoor, G. C. *J. Chem. Soc., Dalton Trans.* **1984**, 1349. (b) Rodiguez-Fortea, A.; Alemany, P.; Alvarez, S.; Ruiz, E. *Chem.—Eur. J.* **2001**, *7*, 627.